Seasonal and interannual variability of nitrate in the eastern Chukchi Sea: Transport and winter replenishment

Calvin W. Mordy[a,b,*], Shaun Bell[a,b], Edward D. Cokelet[b], Carol Ladd[b], Geoff Lebon[a,b], Peter Proctor[a,b], Phyllis Stabeno[b], David Strausz[a,b], Eric Wisegarver[b], Kevin Wood[a,b]

[a]*Joint Institute for the Study of the Atmosphere and Ocean, Box 355672, University of Washington, Seattle, WA 98105-5672, USA*

[b]*Pacific Marine Environmental Laboratory, NOAA, 7600 Sand Point Way, NE, Seattle WA 98115, USA*

*Corresponding author: Tel: (206) 526-6870

E-mail address: mordy@uw.edu (C.W. Mordy)

ABSTRACT

Rapid changes in sea ice and ocean properties are occurring in the Chukchi Sea, and there is considerable uncertainty how these changes might influence nutrient distributions and ultimately primary productivity. Although inorganic nitrogen is a limiting nutrient, there are few reports on seasonal or interannual variability of nitrate, especially those focused on wintertime replenishment of nitrate. This study examined six years of hourly measurements of nitrate at multiple mooring locations off Icy Cape between 2010 and 2018 with a focus on winter replenishment in relation to northward transport. Nitrate concentrations are lowest in newly formed winter water, and rates of local nitrate replenishment appear low relative to the nutrient flux through Bering Strait. There is considerable interannual variability in transport over the northeastern shelf of the Chukchi Sea that is driven by northerly (weakens transport) and southerly (strengthens transport) wind events. Anomalously low nitrate concentrations were observed in the winter of 2011–2012 when transport was negligible, and locally formed, low nitrate winter water remained on the shelf. During winters with the highest transport (2010–2011, 2017–2018), pre-bloom (15 May) nitrate concentrations were high and closely resembled nitrate concentrations in the Bering Sea from the previous fall. In recent years, there has been an increase in southerly wind events. As these conditions enhance total transport and nutrient flux through Bering Strait, contemporary Bering Sea water is advected onto the northern Chukchi Sea shelf. In the presence of southerly wind events, nutrient measurements in the northern Bering Sea in fall can be used to predict pre-bloom nitrate concentrations available for sustaining primary production in the eastern Chukchi Sea the following spring. Since 2005, inorganic nitrogen concentrations in the northern Bering Sea have varied between 11 and 22 µM; an indication that net community production over the eastern Chukchi Sea may have varied between ~30 and 70 g C m^{-2} during this time.

Keywords: Chukchi Sea, Bering Sea, Nitrate, Transport, Replenishment, Nitrate flux, Net community production, NCP

1. Introduction

The Arctic Ocean is undergoing rapid change with warming temperatures and reductions in the extent, thickness and duration of sea ice (Zhang, 2005; Steele et al., 2008; Serreze et al., 2009; Screen and Simmonds, 2010; Cavalieri and Parkinson, 2012; Frey et al., 2015; Wang et al., 2018; Dai et al., 2019). These changes are especially striking in the Chukchi Sea where the open water season continues to increase with the later arrival of ice in fall and earlier ice retreat in spring (Frey et al., 2015; Wang and Overland, 2015; Wood et al., 2015; Serreze et al., 2016; Overland and Wang, 2018; Rolph et al., 2018; Stabeno et al., 2018b; Wang et al., 2018). Lengthening of the open-water season is projected to alter the composition and distribution of phytoplankton communities (Tremblay et al., 2009; Ardyna et al., 2011; Neeley et al., 2018) and the timing and extent of primary production (Arrigo et al., 2008; Hill et al., 2018; Selz et al., 2018; Lewis et al., 2019). These changes are primarily due to increased stratification and a reduction in vertical mixing and diffusion of nutrients from deeper water (30–40 m) into the upper water column. While primary production over the shelf has been tied to the flow of cold, nutrient-rich bottom water (Lowry et al., 2015), to date there are no direct measurements that examine interannual variability of nutrient transport across the eastern shelf of the Chukchi Sea.

The only direct pathway of flow from the Pacific Ocean into the Arctic Ocean is through Bering Strait, a narrow (~80 km), shallow (<55 m) passageway between Siberia and Alaska, which is divided into western and eastern channels by the Diomede Islands (Coachman et al., 1975). Three Pacific water masses enter the Chukchi Sea through Bering Strait: the saline and nutrient-rich Anadyr Water (AW) and Bering Shelf Water (BSW), and the fresher and nutrient-poor Alaskan Coastal Water (ACW) (Coachman et al., 1975). ACW originates primarily on the inner shelf (< 50 m) of the Bering Sea, and includes freshwater inputs from regional rivers including the Yukon River (Woodgate et al., 2005; Aagaard et al., 2006); it generally flows along the eastern side of Bering Strait (Coachman et al., 1975; Danielson et al., 2017). AW originates on the outer shelf or slope of the Bering Sea, and flows through Chirikov Basin (Fig. 1) and along the western side of the strait (Coachman et al., 1975; Danielson et al., 2017).

In Bering Strait, BSW is generally found between ACW and AW (Coachman et al., 1975; Danielson et al., 2017). The primary source of the BSW is the northward flowing current along the 100-m isobath, which is the transition between the middle and outer domains of the Bering Sea (Stabeno et al., 2016b, 2018a). On the northern middle shelf of the Bering Sea, there is substantial interannual variability in nutrient content. For example, there was a significant decline in the concentrations of dissolved inorganic nitrogen (DIN, nitrate + nitrite + ammonium) and phosphate between 2005 and 2016, with concentrations partially rebounding in 2017 (Stabeno et al., 2018a). It is unclear if this variability extends to other portions of the Bering Sea Shelf and slope, or how it might be reflected in BSW that flows across the eastern Chukchi Sea Shelf.

In the Chukchi Sea, nitrogen is the limiting nutrient (Cota et al., 1996, Codispoti et al., 2005, Tremblay et al., 2006), although continual nutrient inputs through Bering Strait (primarily western Bering Strait) make this region analogous to a “chemostat”, and one of the most productive shelves in the Arctic (Sambrotto et al., 1984; Stein and Macdonald, 2004; Hill and Cota, 2005; Sakshaug, 2004; Codispoti et al., 2005, 2013; Hill and Zimmerman, 2010; Hill et al., 2018). Transport through Bering Strait has been measured for decades (Roach et al., 1995; Woodgate et al., 2005, 2012; Woodgate, 2018). The flow is typically northward, and is thought to be driven by a sea level difference (pressure head) between the Pacific and Arctic Oceans (Coachman and Aagaard, 1966; Stigebrandt, 1984; Aagaard et al., 2006) and modified by winds (Aagaard et al., 1985; Coachman and Aagaard, 1988; Roach et al., 1995; Woodgate et al., 2005; Danielson et al., 2017). During the past 25 years, transport through Bering Strait has increased from 0.8 to 1.0 Sv (10^6 m^3 s^{-1}) (Woodgate, 2018), and this was attributed primarily to changes in westward winds along the Arctic coasts and sea-level change in the East Siberian Sea (Peralta-Ferriz and Woodgate, 2017; Woodgate, 2018).

After passing Bering Strait, Pacific Water continues into the central Arctic following three branches (Fig. 1). In the west, flow is toward Herald Canyon, with a portion of the flow exiting Herald Canyon and the remainder turning eastward and remaining on the shelf (e.g. Linders et al., 2017; Li et al., 2019). The Siberian Coastal Current (SCC) flows southwestward along the Siberian Coast with some of the SCC turning northward joining the flow toward Herald Canyon (Linders et al., 2017; Bond et al., 2018). The SCC appears intermittent and is forced by wind and buoyancy (Weingartner et al., 1999), and some of the SCC has been observed to flow southward into the western channel of Bering Strait (Roach et al., 1995; Weingartner et al., 1999). In the east, the Alaskan Coastal Current (ACC) flows northeastward along the Alaskan coast toward Barrow Canyon (Weingartner et al., 1998). BSW flows north through Central Channel with the majority of flow joining the ACC just north of Icy Cape; most of this flow exits through Barrow Canyon (Stabeno et al., 2018b).

As water flows through the Chukchi Sea, physical characteristics are seasonally modified through ice melt and ice formation (i.e. brine exclusion), and warming and cooling. Temperature and salinity signatures have been used to define seasonal water types in the Chukchi Sea including ACW, melt water (MW), summer water (SW), and winter water (WW), and used to identify the presence of saltier Atlantic Water (AtlW), which can upwell along the shelfbreak (Gong and Pickart, 2015; Ladd et al., 2016; Danielson et al., 2017).

From 2010 to present, moorings have been deployed along the Icy Cape line (Fig. 1) providing time series of transport, nitrate, and other variables on the eastern shelf (Ladd et al., 2016; Stabeno et al., 2018b). Transport along the Icy Cape line is likely a combination of ACW near the coast and BSW farther offshore, which converge near Icy Cape (Fig. 1). There is considerable short-term variability in the time series due to local wind forcing and likely remote wind forcing (Danielson et al., 2014, 2017), as the transport and winds are significantly correlated (Stabeno et al., 2018b). While the variability in flow is dominated by the winds, monthly mean transport at Icy Cape shows a seasonal signal similar to Bering Strait with transport weakest in fall and winter (Stabeno et al., 2018b). The flow at Icy Cape accounts for ~40% of annual transport through Bering Strait, although this fraction varies on seasonal and interannual time scales (Stabeno et al., 2018b).

Several high-resolution nitrate time series have been reported on the Chukchi Shelf (Ladd et al., 2016; Hauri et al., 2018), but heretofore there has not been a study on the seasonal and interannual variability of nitrate over the shelf that includes winter replenishment. Herein, we present several years of continuous nitrate measurements at the Icy Cape mooring sites (C1, C2, C3; Fig. 1). While nitrate concentrations are modulated by numerous factors, including nitrification (oxidation of ammonium into nitrate), denitrification (nitrate reduction into nitrogen gas), brine exclusion, and primary production, this study is focused on seasonal and interannual variability, and winter replenishment in relationship to the transport of nutrients across the shelf.

2. Methods

2.1. Shipboard Hydrography

Each year (2010–2018), hydrographic transects were run along the Icy Cape transect line in August or September in conjunction with mooring deployment and recovery. Profile data were collected using a Sea-Bird SBE 911plus Conductivity, Temperature, and Depth (CTD) instrument with dual temperature and salinity sensors. CTD data were recorded during the downcast, with a descent rate of 15 m min^{-1} to a depth of 30 m, and 30 m min^{-1} below that. Discrete calibration samples for salinity were collected from Niskin bottles on approximately one third of the casts on the transect line and also at the mooring sites. The samples were analyzed on a laboratory salinometer at the NOAA Pacific Marine Environmental Laboratory (PMEL) in Seattle, Washington. During hydrographic transects, discrete nutrient samples were collected from Niskin bottles at the surface, at 10-m intervals throughout the water column, and at the bottom of the cast. At the mooring sites, discrete nutrient samples were collected at the deployment depth of the nitrate sensor during mooring recovery and redeployment and used for calibration. Additional *in situ* calibration samples were collected opportunistically at other times while the nitrate sensors were deployed. Nutrient samples were filtered through 0.45 µm cellulose acetate filters, and frozen for later analysis at PMEL. Nitrate was measured using automated continuous flow analysis with a segmented flow and colorimetric detection. Standardization and analysis procedures specified by Gordon et al. (1994) were closely followed including calibration of labware, preparation of primary and secondary standards, and corrections for blanks and refractive index. In this method, nitrate+nitrite and nitrite are both measured, and nitrate is determined from the difference.

2.2. Moorings

Moorings have been deployed at three sites offshore of Icy Cape since August 2010 (C1, C2, and C3; Table 1, Fig. 1) with sensors located 4-6 m off the bottom. Measurements at each site included chlorophyll fluorescence (Sea-Bird/WetLabs ECO fluorometer), temperature and salinity (Sea-Bird SBE16), and current speed and direction (Aanderaa RCM-9, SeaGuard and/or Teledyne RD Instruments acoustic Doppler current profiler [ADCP], 300 or 600 kHz) (Stabeno et al., 2018b). Mooring data were collected at least hourly. The Sea-Bird ECO fluorometers, Sea-Bird SBE16s, and current meters were calibrated prior to deployment, and the data were processed according to manufacturers' specifications. Unless otherwise indicated, all current meter and salinity time series were low-pass filtered with a 35-h, cosine-squared, tapered Lanczos filter to remove higher-frequency variability, and resampled at 6 h intervals. Final processed time series were accurate to ± 0.0005 S m^{-1} and ± 0.5 cm s^{-1} for salinity and currents, respectively. At mooring site C2, the drift in the salinity of the moored SBE16 was usually minimal (<0.1) when compared to discrete samples collected from shipboard hydrographic CTD casts at the mooring site that are used for salinity calibration.

Nitrate sensors (Sea-Bird/Satlantic ISUS or SUNA) have been deployed at C2 each year, and were occasionally deployed at C1 and C3. In 2012 and 2013, the nitrate sensors deployed at C2 did not record data. To reduce biofouling, the SUNA instruments had a wiper that was activated prior to each set of hourly measurements, and the ISUS instruments were plumbed into the outflow of a Sea-Bird SBE-16 with anti-fouling agents mounted on either side of the ISUS flow cell. To ensure that the SBE-16 pump was triggered before the ISUS began sampling, the ISUS sampled 3 minutes after the pump was activated.

The hourly nitrate data included a dark frame (or reference sample) and 10–15 samples of nitrate (the number of samples has varied over the years). Each sample included the full spectrum of 255 spectrometer channels between ~ 200 and 400 nm, and an estimate of nitrate based upon the absorbance of ~35 spectrometer channels between 217 and 240 nm. The SUNA also provided several channels to assess potential interference from other absorbers (e.g. colored dissolved organic matter) including the absorbance at 254 and 350 nm, which was outside the absorbance range of nitrate, and the root-mean-square error between the measured and standard absorbance curves.

Spectral plots were used to assess performance of each instrument and identify data dropouts (Supplementary Fig. S1). The SUNA generally outperformed the ISUS as the SUNA had fewer data dropouts, and the spectral intensity of the SUNA was relatively strong throughout the deployment. This result was most likely due to the use of an optical wiper on the SUNA. Data processing included de-spiking by identifying deviations at 254 nm or 350 nm, calibration (discussed below), and applying a 35 h, cosine-squared, tapered Lanczos filter to remove tidal and higher-frequency variability.

The ISUS and SUNA optical nitrate sensors have a reported accuracy of ~2 µM, and do not have internal standards. Based upon numerous deployments since 2001, while these sensors provide relative changes in nitrate concentrations on tidal to seasonal scales (Mordy et al., 2005, 2019), absolute values are unreliable and the sensors must be calibrated against discrete field samples collected while the sensors are deployed. Each moored dataset was calibrated by determining the difference between the moored and discrete data at each calibration point, then regressing these differences against the discrete sample time to correct for sensor drift. During the deployment at C2 in 2010–2011, the ISUS often recorded negative values and the sensor failed in July 2011, eliminating the possibility of an *in-situ* calibration from the recovery CTD cast. In this instance, the calibration drift correction used the initial *in-situ* calibration point and the most negative daily mean value (observed on 12 June), which was set to zero. The resulting pattern was similar to the nitrate time series at C1, which had a double maximum between late March and late May, and ~ 9 µM drop in nitrate on 4–7 June (not shown). After calibration, the C2 time series 2016–2017 had periods of negative values. For this time series, a secondary drift correction was applied by setting the most negative daily mean value (observed on 14 November) to zero.

2.3 Transport

Estimates of total transport were obtained as described in Stabeno et al. (2018b). This approach was used to calculate transport of the ACC in the Gulf of Alaska (Schumacher et al., 1989; Stabeno et al., 1995, 2016a) and the Alaskan Stream (Stabeno and Hristova, 2014). Transport was calculated from current measurements along a line of moorings (C1, C2, C3) across the region of interest. Using low-pass filtered currents, the component of velocity perpendicular to the mooring line was calculated. The normal component of velocity at each current meter or ADCP bin was multiplied by the cross-sectional areas. The horizontal distance of the cross-sectional area was the midpoint between two adjacent moorings, the distance between the mooring and the shore, or the outer edge of the mooring line was defined as the same half distance as between the outer mooring and its nearest neighbor (as appropriate). The vertical boundaries were the surface, the bottom at the mooring site, or the halfway point between instruments/bins, as appropriate. The individual mooring transport time series were summed across the section. In the Chukchi Sea, this method was reliable when all three moorings (C1, C2, and C3) provided current measurements. When data from one mooring were missing, the transport was calculated by selecting a calculated transport (T) when all three moorings provided data (data set D), removing the comparable missing velocities from D, and doing a multiple linear regression of the more limited data set on the transport, T. We then used the regression parameters to calculate transport for the years when there were missing velocities. See Table 3 in Stabeno et al. (2018b) for more detailed explanations.

2.4 Other Measurements

Daily sea-ice concentrations at 25-km resolution were generated using the Advanced Microwave Scanning Radiometer - Earth Observing System (AMSR-E) Bootstrap Algorithm (Comiso, 2017), and are available from the National Snow and Ice Data Center (https://nsidc.org/data/nsidc-0079/versions/3). Time series of percent areal coverage were calculated in 50 km × 50 km boxes around each of the mooring sites (Fig. 1).

Wind velocity was obtained from the North American Regional Reanalysis (NARR) using the nearest gridpoint to the C2 mooring site. NARR was introduced as an extension to the National Centers for Environmental Prediction (NCEP) Reanalysis 2 (NCEPR2) for the North American Region using the high resolution NCEP Eta model (~32 km grid size compared to NCEPR2's 2.5° grid) and includes additional assimilated parameters to improve the reanalysis product (Mesinger et al., 2006). NARR winds are available at 3 hourly intervals and monthly averages were used for this study.

Several classifications of water types have been presented in the literature (Gong and Pickart, 2015; Danielson et al., 2017, this issue). Here we use the Danielson et al. (2017)

classification scheme modified by Ladd et al. (2016) to identify water influenced by brine exclusion (Table 2).

3. Results

3.1. C2 Time Series

Time series shown in Fig. 2 include sea-ice extent, classification of the bottom water mass, salinity, and concentrations of nitrate and chlorophyll-a at the C2 mooring for deployments in 2010, 2011, and 2014–2017. Moorings were deployed in mid-to-late summer at a time when the bottom water at C2 was primarily SW. The fall transition from SW to WW occurred prior to the arrival of ice (except for a brief appearance of ice in 2016), and WW persisted for ~2 months after ice retreat, except in 2011 with the arrival of warmer water for a short period soon after ice retreat.

Increases and decreases in nitrate and salinity often corresponded on event and seasonal scales. Event-scale variability is evident in the December–January time series in 2010–2011, 2011–2012, 2014–2015, and 2015–2016. Other notable events include increased nitrate and salinity on 1 November 2010, 22 October 2014, and 10 November 2014, which are related to the presence of AtlW and coastal polynyas (AtlW was observed at C1 on 10 November 2014) (Ladd et al., 2016). Other event-scale changes in salinity were not reflected in nitrate (e.g. mid-May 2012 and late February–March 2015).

Corresponding seasonal trends in nitrate and salinity included the fall transition and winter replenishment. During the fall transition, freshening and a reduction of nitrate concentrations in bottom water were common with the lowest values typically occurring in November–December. Exceptions were in October–November 2010, when salinity and nitrate increased likely due to a weak upwelling event of AtlW (Ladd et al., 2016), and the 2014 polynya events mentioned above. Winter replenishment of nitrate typically occurred between January and May. In January–May of 2011, 2016, and 2017, there was a corresponding increase in salinity and nitrate. During other years, replenishment was more variable. In 2012, winter replenishment of nitrate did not begin until April. In January–June 2015, salinities were variable but showed no seasonal trend, while nitrate steadily increased through the winter. In 2018, although salinity was variable without a considerable seasonal trend, nitrate concentrations were high through the winter reaching 24 µM in late March.

To assess interannual variability in wintertime nutrient replenishment, nitrate and salinity anomalies were determined for January–May (Fig. 3). The multi-year (2011, 2012, 2015–2018) hourly means of nitrate and salinity that were used to calculate anomalies are shown in Fig. 3a. Mean nitrate did not include data from 20-31 May 2018, as there was a sharp decline in nitrate associated with an early ice retreat and high levels of chlorophyll (Fig. 2f, Stabeno et al., this issue). In the mean, nitrate and salinity were significantly correlated ($R^2 = 0.83$, $p < 0.0001$) with values generally increasing from January–May (Fig. 3a). While there was frequent correspondence between nitrate and salinity anomalies (e.g. early January 2018, February–April 2015, January–May 2017), at other times anomalies were of opposite sign (e.g. January 2011, May 2012). Most notable was the negative nitrate anomaly in 2012 and the positive nitrate anomaly from mid-January to mid-May 2018, both accompanied by relatively neutral salinity anomalies. The second largest positive nitrate anomaly occurred in March–May 2011. These positive nitrate anomalies were evident in the wintertime nitrate–salinity relationship (Fig. 4) wherein nitrate concentrations in 2011 and 2018 more closely resembled data from the Bering Sea, and were significantly higher ($p < 0.0001$) than in other years that had maximum nitrate concentrations generally <13 μM.

In spring, the timing of nitrate drawdown in bottom waters at C2 was related to ice retreat and/or increased chlorophyll concentrations (Fig. 2), but varied among the years (Stabeno et al., this issue). In June 2011, there was a sharp drop in nitrate coincident with ice retreat despite relatively low chlorophyll concentrations. In the summers of 2015 and 2017, the drawdown of nitrate occurred within a month of ice retreat coincident with relatively high chlorophyll concentrations. In summer 2016, winter water persisted until September while chlorophyll concentrations remained relatively low; nitrate concentrations slowly declined through the seasons with minimum concentrations occurring in November (observed in the subsequent deployment time series, Fig. 2e). In May–June 2018, while there was an initial reduction in nitrate associated with ice retreat and a chlorophyll peak, several pulses of ice and nitrate occurred thereafter. A similar increase in nitrate was observed in July 2011 absent ice cover. Both instances were associated with WW. In 2012, ice lingered at C2 until late July as nitrate concentrations increased from May–July.

3.2. Icy Cape time series

Time series of nitrate, salinity, and areal ice coverage at the three moorings along the Icy Cape line (C1, C2, and C3) are shown for 2016–2017 (Fig. 5a-c) and 2017–2018 (Fig. 5d-f).

While episodic and seasonal variability were similar among the three moorings in individual years, there was considerable interannual variability. In the 2016–2017 time series, salinities freshened by ~1 in November 2016, and the freshest bottom water was observed in late December 2016 and January 2017 (Fig. 5a-c). Between January and August 2017 salinities increased to ~ 32.8 with a freshening event occurring in May and June 2017. In the 2016–2017 nitrate time series, the fall transition was similar at the three moorings with increased nitrate in mid-October 2016 followed by a minimum in November that occurred several weeks prior to the appearance of winter water. There was less correspondence among the three moorings during winter replenishment as concentrations at C1 showed step increases in January and March with concentrations of 11 µM in April; concentrations at C2 increased to 5 µM in January followed by a relatively steady increase to 13 µM in June; and concentrations at C3 steadily increased from the minimum in November to 16 µM in May. At all three moorings, nitrate concentrations declined to < 5 µM in June 2017 concomitant with ice retreat and increasing chlorophyll concentrations in the bottom water, and nitrate drawdown was more gradual at C1 compared to C2 and C3.

In the 2017–2018 salinity time series at C1, C2, and C3 (Fig. 5d-f), freshening associated with the fall transition and the replenishment of salt during winter were less pronounced than in the 2016–2017 time series. Increased salinity at C1 on 17–18 December 2017, was associated with upwelling of warmer AtlW, an event that slightly warmed temperatures at C2 (17–18 December mean temperature = -0.8°C) and formed a hybrid latent/sensible heat polynya (Ladd et al., 2016) with evidence of brine exclusion (salinity > 33.6) observed at all three moorings (Fig. 6).

Nitrate concentrations at the three moorings were low in October 2017 and rapidly increased in November and December during the transition from SW to WW. Variability in nitrate was high in December 2017 concomitant with the polynya, and also in February–March 2018 with stepwise increases occurring in March. Prior to ice retreat, nitrate concentrations of 15 – 20 μM were observed at the three moorings. Nitrate concentrations rapidly declined upon ice retreat and increased bottom chlorophyll concentrations (Stabeno et al., this issue).

Anomalies for salinity and nitrate at the three moorings (Fig. 7) were determined for January – May using the mean values derived at C2 and employed in Fig. 3. In 2017, salinity anomalies were negative at all three moorings while the nitrate anomalies had greater spatial and temporal variability. At C1, the 2017 nitrate anomaly was positive in January, and negative in the remaining months with the seasonal drawdown of nitrate beginning in mid-May 2017 (Fig. 5a). At C2, nitrate and salinity anomalies were negative. At C3, the 2017 nitrate anomaly was generally neutral or positive with the highest anomalies observed in mid-April – May. In 2018, salinity anomalies were neutral except for the high salinities observed in early January that were associated with a polynya (Fig. 6). The highest nitrate anomalies at all three moorings were observed in February–April, interrupted by lower values generally associated with negative salinity anomalies.

3.3. Transport and pre-bloom nitrate concentrations

Interannual variability in transport across the shelf during winter is captured by comparing 3-month means of transport across the Icy Cape line (Fig. 8). Weak or negative transport was observed in winters spanning 2011–2012 to 2015–2016 with the weakest mean transport in 2011–2012. Moderate transport was observed in 2016–2017 and relatively high transport was observed from December 2010 to April 2011 and in the fall 2017 to winter 2018.

In years with weak transport, relatively low nitrate concentrations were observed at the C2 mooring from January–May (Fig. 4, green) indicating that early in the year the northern shelf may retain a remnant nutrient signature from the previous summer. In a year with moderate transport (Fig. 8a, 2016–2017), water with a stronger Bering Sea signature was observed in May 2017 at the C3 mooring (salinity = 32.3, NO_3 = 15.5 µM; Fig 5c) , while C1 and C2 appeared to retain older water (NO_3 < 13 µM; Fig. 5a, b). This result implies that in 2017, transport through the central channel exceeded flow farther inshore, assuming all other processes being equal (e.g. brine exclusion, nitrification, and denitrification). This is consistent with findings that BSW flows through Bering Strait and northward through Central Channel, reaching C3, then C2 and finally C1 (unpublished data). In years with the largest monthly mean transports, water with a Bering Sea signature (i.e. NO_3 = 15–20 µM) was observed from January–May 2011 at C2 (Fig. 4, orange) and at all three moorings in 2017–2018 (Fig. 4, red, and Fig. 5d-f).

Given the correspondence along the Icy Cape line between high levels of multi-month mean transport and the appearance of water with Bering Sea characteristics, a comparison was made between pre-bloom nitrate content and transport (Fig. 9). Mean transport in January through May was compared to the 3-day mean nitrate concentration centered on 15 May (black symbols in Fig. 9). Note, 15 May was prior to major ice retreat at any of the C2 mooring time series and prior to large accumulations of bottom chlorophyll (Fig. 2). The regression slope in Fig. 9 was not significant ($p = 0.08$, $F = 5.4$). Most notable were the discrepancies in 2017 between relatively high-transport/low-nitrate concentrations, and the very low nitrate concentrations in 2012.

In 2012, 2015, and 2017, after 15 May, nitrate concentrations in WW continued to increase at C2 for weeks to months despite ice retreat and the accumulation of chlorophyll in bottom water (Fig. 2). This is illustrated in a second comparison between nitrate and transport in Fig. 9 (blue symbols). This comparison shows the maximum 3-day mean nitrate concentrations between 15 May and July in each of these years compared to the prior 5-month mean of transport. For example, in 2012, the maximum 3-day mean nitrate between May and July was 15.3 µM and occurred on 27 July 2012, and the mean 5-month transport from March–July was 0.37 Sv. While neither of the regression slopes in these comparisons were significant, these results illustrate that in some years, there is a continual flux of cold nitrate-rich WW over the shelf through spring and into summer (blue arrows in Fig. 9), seasons when contributions from nitrification are thought to be low (Baer et al., 2017).

In summer and fall, there is considerable variability in DIN concentrations near the M8 mooring on the northern middle shelf of the Bering Sea (Stabeno et al., 2018a). In the proximity of the M8 mooring (62.194°N, 174.688°W), concentrations of DIN in bottom water declined by ~37% between 2005 and 2016 before recovering in 2017 and 2018 (Stabeno et al., 2018a; Fig. 10a). The mechanisms forcing this variability are still undetermined. In winter, this water begins to flow over the Chukchi Shelf, and during this transit ammonium is likely nitrified and contributes to the nitrate pool (Baer et al., 2017). In the absence of primary production in winter, we might expect correspondence between summer/fall DIN concentrations at M8 in the northern Bering Sea and pre-bloom (15 May) nitrate concentrations at C2 in the Chukchi Sea the following spring (Fig. 10b). For example, the lowest values in the northern Bering Sea were observed in September 2016 (Fig. 10a), and likely resulted in the low values observed spring 2017 in the Chukchi Sea despite relatively high transport (Fig. 9). Arrigo et al. (2017) surveyed the northeastern Chukchi Sea in May–June 2014 and reported a mean pre-bloom nitrate concentration in bottom water of 14.0 ± 1.9 µM. Although DIN was not measured at M8 the previous year, their finding is consistent with regressed concentration for 1 October 2013 (14.0 µM, orange data in Fig. 10). While consistent in the mean, they observed higher concentrations in the central channel and lower concentrations near the shelf break.

While there is nearly a 1:1 correspondence between summer/fall DIN in the Bering Sea and pre-bloom nitrate in the Chukchi Sea (black symbols in Fig. 10b), there was a large discrepancy at C2 in 2012. Despite relatively high concentrations of DIN in the Bering Sea, the winter of 2012 had the largest negative nitrate anomaly (Fig. 3c), and nitrate replenishment that year did not begin until April (Fig. 2b). These results are explained by the absence of transport across the Icy Cape line between September 2011 and May 2012 (Fig. 8). The discrepancy is much smaller on 27 July 2012 when maximum 3-day mean nitrate concentrations were observed (blue symbols in Fig. 10b); that is when water with Bering Sea characteristics arrived at Icy Cape. In 2015 and 2017, nitrate concentrations continued to increase after 15 May, and the maximum 3-day mean nitrate concentrations were greater than observed in the Bering Sea (Fig. 10b). These higher nitrate levels may be the result of ammonification-nitrification, brine rejection, or mixing with AW upstream of the Icy Cape line in winter.

4. Discussion

The seasonal water masses in the Chukchi Sea are typically defined by temperature and salinity, and the seasonal progression of these water masses over the shelf are well described

(Woodgate et al., 2005; Gong and Pickart, 2015; Lowry et al., 2015; Danielson et al., 2017; Lin et al., 2019; Danielson et al., this issue). In spring and summer, WW is gradually replaced from south to north by MW, SW, and ACW (Lowry et al., 2015; Lin et al., 2019; Danielson et al., this issue) due to the seasonal progression of ice melt across the shelf and enhanced transport in summer forced by southerly winds (Woodgate et al., 2005; Stabeno et al. 2018b). During hydrographic surveys conducted in mid-to-late-summer, conditions off Icy Cape are typified by a strong two-layer system (Fig. 11). The surface layer is composed of ACW, SW, and/or MW, and is relatively fresh, warm, and nitrate-poor (Fig. 11; Danielson et al., 2017). In the bottom layer, WW and SW are the primary water types found off Icy Cape in summer, and their relative contributions depend in part on the timing of sampling (Lin et al., 2019). While SW is nutrient-poor, WW has moderate nitrate content in late summer (Lowry et al., 2015; Danielson et al., 2017, Lin et al., 2019), and this water type is thought to initiate and sustain phytoplankton blooms throughout the growing season (Lowry et al., 2015).

By October, most of the WW along the bottom has been flushed off the shelf by relatively warm ACW and SW (Lin et al., 2019; Danielson et al., this issue). During the fall transition, storms break down the two-layer system that is prevalent in summer, and mix warmer, fresher, and nutrient-poor water to depth (Fig. 12; Woodgate et al., 2005; Nishino et al., 2016). As a result, bottom salinities and nutrient concentrations are often lowest during this period (Figs. 2, 5, and 12). Exceptions to this pattern along the Icy Cape line include fall 2010 and 2014 when upwelling events in Barrow Canyon transported salt and nitrate over the shelf (Fig. 2; Ladd et al., 2016). The transition from SW to WW generally occurred in September–November prior to the arrival of ice. In 2016, there was a short period of ice cover during the fall transition, and, in 2016 and 2017, SW was evident through November (Fig. 2). This transition may be further delayed with future warming (Wood et al., 2018; Danielson et al., this issue). The rapid rates of heat loss over the shelf (e.g. Wood et al., 2018; Danielson et al., this issue) signify that the transition to WW is primarily a local or regional event rather than advective event (Lowry et al., 2015). Thus, when formed, WW is relatively fresh and nutrient poor (Figs. 2 and 5; Woodgate et al., 2005; Lowry et al., 2015).

Replenishment of nitrate over the shelf in winter occurs through brine exclusion (Aagaard et al., 1981; Anderson et al., 1988), nitrification, which has the highest rates in winter (Christman et al., 2011; Baer et al., 2017), upwelling along the shelf break (Ladd et al., 2016) and the transport of nutrients through Bering Strait (Walsh et al., 1989; Springer and McRoy, 1993), and is modulated by denitrification (Chang and Devol, 2009). In terms of nutrient transport, the majority of water flowing over the eastern Chukchi Sea Shelf has its origins from the middle and outer shelf of the northern Bering Sea (Stabeno et al., 2016b). While winter nutrient concentrations in the northern Bering Sea are rarely measured, bottom water concentrations in spring and summer/fall in the Bering Sea are similar and relatively high compared to recently formed (October – November) WW in the Chukchi Sea (Table 3; Figs. 2 and 5).

Despite the relatively high nutrient concentrations in Bering Sea source waters, transport across the eastern Chukchi Sea Shelf in winter is weak and highly variable due to prevailing northerly winds that can sometimes result in southward transport (Stabeno et al., 2018b). Along the Icy Cape line, while there are periods of strong northeastward transport in fall and winter (e.g. February 2011), 5 to 20-day periods of southwestward transport are not uncommon (see Fig. 12 in Stabeno et al. 2018b). They found that while ~40% of the annual flow through Bering Strait passes the Icy Cape line, less than a fifth of this transport occurs during December–April. This is an indication that, on the eastern shelf, advective replenishment of nitrate in winter may be sporadic, and highly variable among years. Model results suggest that in the first 180 days of the year, the southern shelf of the Chukchi Sea (south of ~70°N) is filled with water that has recently (< 5 mo) passed through Bering Strait (Spall, 2007), thereby introducing relatively high concentrations of nutrients from the Bering Sea into the southern Chukchi Sea. These model results also suggest that, early in the year, the northern shelf in the Chukchi Sea may retain older water (Spall, 2007), a result supported by the low nutrient-salinity relationships in Fig. 4 relative to Bering Sea water. This is also consistent with a May-June 2014 survey that observed lower nitrate concentrations on the northern shelf (Arrigo et al., 2017).

Macdonald et al. (2010) provided a mean estimate annual new production in the Chukchi Sea of 50 g C m^{-2} y^{-1} (5 to 160 g C m^{-2} y^{-1}) with a corresponding annual mean nitrogen demand of 12.4 kmol N s^{-1}. Their estimate of Pacific inflow of DIN through Bering Strait was 16.5 kmol N s^{-1}. Torres-Valdés et al. (2013) used inverse modeled velocities and a July 2005 nitrate section that crossed the entire southern Chukchi Sea and determined a summertime nitrate flux of 9 ± 0.8 (± SD) kmol N s^{-1} with most of this flux occurring in the western Chukchi Sea. For contrast, a summary of monthly wintertime winds, transport, and nitrate flux in the northeastern Chukchi Sea are presented in Fig. 13. In November–April, the nitrate flux in the northeastern Chukchi Sea ranged from < 1.5 kmol N s^{-1} in winters with weak transport (i.e. 2011–2012, 2014–2015, 2015–2016) to 10 kmol N s^{-1} in winters with high transport (Fig. 13). Higher transports were associated with more easterly or southerly winds, and higher fluxes generally occurred in late winter or early spring (May) as northerly winds weakened and contemporary water from the Bering Sea spread across the northeastern Chukchi Sea. The low nitrate flux in May 2012 reflected the weak transport of remnant winter water that had yet to be flushed from the region (Fig. 10b).

The wintertime nitrate flux on the northeastern shelf was often low relative to the findings of Macdonald et al. (2010) and Torres-Valdés et al. (2013). In most years contemporary water from the Bering Sea arrived at the Icy Cape line in early spring (Fig. 10b) and was perhaps modified in route from nitrate-rich AW, nitrification, or denitrification. During the growing season, nitrate in bottom water was often consumed (Fig. 2), reinforcing the notion that nitrate is the primary limiting nutrient (Cota et al., 1996; Codispoti et al., 2005; Tremblay et al., 2006; Lowry et al., 2015) and enabling an estimate of net community production (NCP) upstream of the Icy Cape line (i.e. the seasonal change in carbon or nutrients that represents production minus community respiration). Defining pre-bloom nitrate concentrations as 15 May or later (nitrate concentrations continued to increase in 2012, 2015, and 2017), concentrations at the C2 mooring range from 12.0 ± 0.3 (± SD) µM in 2016 to 16.7 ± 0.2 µM in 2011 (Fig. 10b). This corresponds to NCP of 35 – 48 g C m^{-2} (assuming consumption to 40 m and a C:N ratio of 6 from Hansell et al., 1993).

Arrigo et al. (2017) measured pre-bloom nitrate concentrations in the northeast Chukchi Sea in 2014, and derived NCP values of 27.8 ± 4.1, 37.6 ± 5.6, and 42.3 ± 6.9 g C m^{-2} y^{-1} for nitrate consumption to 30, 40, and 50 m, respectively. Their estimates were generally lower than prior studies in the region (40–70 g C m^{-2} y^{-1}; Hansell et al., 1993; Codispoti et al., 2013; Mills et al., 2015). They argued that earlier estimates were unreasonably high because pre-bloom nitrate concentrations were not locally and/or rigorously determined; for example, Hansell et al. (1993) employed nitrate data from the southeast Bering Sea without consideration of denitrification over the Bering Sea shelf. Given that: i) nitrate consumption may extend to at least 40–45 m; ii) pre-bloom concentrations at C2 correspond to fall concentrations at M8 (Fig.

10b); and iii) DIN at M8 varies from ~11 to 22 μM (Fig 10a), it is reasonable to expect NCP upstream of C2 to vary interannually between ~30 and 70 g C m^{-2} y^{-1}.

5. Conclusion

As WW warms in spring and summer to > -1.6°C, it has been categorized as remnant winter water (Gong and Pickart, 2015; Lin et al., 2019). This definition does not distinguish between water advected through Bering Strait during winter and remnant summer water that has locally cooled, transitioned into winter water, and, in some years, is still residing over the northern shelf. This distinction is important because nitrate concentrations are lowest in newly formed WW, and rates of local nitrate replenishment appear low relative to the nutrient flux through Bering Strait. In recent years there has been an increase in southerly wind events (Stabeno, 2019; Stabeno and Bell, 2019) that may be reinforced by warming of arctic shelves (Tachibana et al., 2019; Danielson et al., this issue). These conditions enhance total transport and nutrient flux through Bering Strait, and introduce contemporary Bering Sea water into the northern Chukchi Sea shelf. As a result, in the presence of southerly wind events, nutrient measurements at the M8 mooring in the Bering Sea from the prior summer/fall should make it possible to predict pre-bloom nitrate concentrations available for sustaining primary production in the eastern Chukchi Sea. Since 2005, annual summer/fall DIN concentrations at M8 in the Bering Sea have varied between 11 and 22 μM (Fig. 10), an indication that NCP over the eastern Chukchi Sea may have varied by 50% during this time.

Acknowledgements

This is contribution No. 5016 for Pacific Marine Environmental Laboratory, contribution No. 2019-1024 for JISAO, and contribution No. EcoFOCI-0935 for NOAA's Ecosystem Fisheries Oceanography Coordinated Investigations. We thank the officers, captains and crew of the USCGC *Healy*, NOAA Ships *Oscar Dyson* and *Ronald H. Brown*, the R/Vs *Aquila* and *Ocean Starr*, and F/V *Mystery Bay*. We thank W. Floering, N. Kachel, and M. Langis for assistance with field operations, M. Sullivan for archival of data and metadata, and S. Bigley, M. Lomas and several anonymous reviewers for comments that greatly helped to improve this manuscript.

Funding: This work was supported by the National Oceanic and Atmospheric Administration; the Bureau of Ocean Energy Management CHAOZ, CHAOZ-X, and ArcWEST programs; the NPRB Arctic Program (A92-02a, A92-02b); and the Joint Institute for the Study of the Atmosphere and Ocean (JISAO) under NOAA Cooperative Agreement NA15OAR4320063.

References

Aagaard, K., Coachman, L.K., Carmack, E., 1981. On the halocline of the Arctic Ocean. Deep-Sea Res. Part A-Oceanogr. Res. Pap. 28(6), 529–545. https://doi.org/10.1016/0198-0149(81)90115-1

Aagaard, K., Roach, A.T., Schumacher, J.D., 1985. On the wind-driven variability of the flow through Bering Strait. J. Geophys. Res.-Oceans 90(C4), 7213–7221. https://doi.org/10.1029/JC090iC04p07213

Aagaard, K., Weingartner, T.J., Danielson, S.L., Woodgate, R.A., Johnson, G.C., Whitledge, T.E., 2006. Some controls on flow and salinity in Bering Strait. Geophys. Res. Lett. 33(19), L19602. https://doi.org/10.1029/2006GL026612

Anderson, L.G., Jones, E.P., Lindegren, R., Rudels, B., Sehlstedt, P.I., 1988. Nutrient regeneration in cold, high salinity bottom water of the Arctic shelves. Cont. Shelf Res. 8(12), 1345–1355. https://doi.org/10.1016/0278-4343(88)90044-1

Ardyna, M., Gosselin, M., Michel, C., Poulin, M., Tremblay, J.É., 2011. Environmental forcing of phytoplankton community structure and function in the Canadian High Arctic: Contrasting oligotrophic and eutrophic regions. Mar. Ecol. Prog. Ser. 442, 37–57. https://doi.org/10.3354/meps09378

Arrigo, K.R., Mills, M.M., van Dijken, G.L., Lowry, K.E., Pickart, R.S., Schlitzer, R., 2017. Late spring nitrate distributions beneath the ice-covered northeastern Chukchi Shelf. J. Geophys. Res. Biogeosci. 122(9), 2409–2417. https://doi.org/10.1002/2017JG003881

Arrigo, K.R., van Dijken, G., Pabi, S., 2008. Impact of a shrinking Arctic ice cover on marine primary production. Geophys. Res. Lett. 35(19), L19603. https://doi.org/10.1029/2008GL035028

Baer, S.E., Sipler, R.E., Roberts, Q.N., Yager, P.L., Frischer, M.E., Bronk, D.A., 2017. Seasonal nitrogen uptake and regeneration in the western coastal Arctic. Limnol. Oceanogr. 62(6), 2463–2479. https://doi.org/10.1002/lno.10580

Bond, N., Stabeno, P., Napp, J., 2018. Flow patterns in the Chukchi Sea based on an ocean reanalysis, June through October 1979–2014. Deep-Sea Res. Part II-Top. Stud. Oceanogr. 152, 35–47. https://doi.org/10.1016/j.dsr2.2018.02.009

Cavalieri, D.J., Parkinson, C.L., 2012. Arctic sea ice variability and trends, 1979–2010. Cryosphere 6(4), 881–889. https://doi.org/10.5194/tc-6-881-2012

Chang, B.X., Devol, A.H., 2009. Seasonal and spatial patterns of sedimentary denitrification rates in the Chukchi Sea. Deep-Sea Res. Part II-Top. Stud. Oceanogr. 56(17), 1339–1350. https://doi.org/10.1016/j.dsr2.2008.10.024

Christman, G.D., Cottrell, M.T., Popp, B.N., Gier, E., Kirchman, D.L., 2011. Abundance, diversity, and activity of ammonia-oxidizing prokaryotes in the coastal Arctic Ocean in summer and winter. Appl. Environ. Microbiol. 77(6), 2026–2034. https://doi.org/10.1128/AEM.01907-10

Coachman, L.K., Aagaard, K., 1966. On the water exchange through Bering Strait. Limnol. Oceanogr. 11(1), 44–59. https://doi.org/10.4319/lo.1966.11.1.0044

Coachman, L.K., Aagaard, K., 1988. Transports through Bering Strait: Annual and interannual variability. J. Geophys. Res.-Oceans 93(C12), 15535–15539. https://doi.org/10.1029/JC093iC12p15535

Coachman, L.K., Aagaard, K., Tripp, R.B., 1975. Bering Strait: The Regional Physical Oceanography. University of Washington Press, Seattle, WA.

Codispoti, L.A., Flagg, C., Kelly, V., Swift, J.H., 2005. Hydrographic conditions during the 2002 SBI process experiments. Deep-Sea Res. Part II-Top. Stud. Oceanogr. 52(24-26), 3199–3226. https://doi.org/10.1016/j.dsr2.2005.10.007

Codispoti, L.A., Kelly, V., Thessen, A., Matrai, P., Suttles, S., Hill, V., Steele, M., Light, B., 2013. Synthesis of primary production in the Arctic Ocean: III. Nitrate and phosphate-based estimates of net community production. Prog. Oceanogr. 110, 126–150. https://doi.org/10.1016/j.pocean.2012.11.006

Comiso, J.C., 2017. Bootstrap Sea Ice Concentrations from Nimbus-7 SMMR and DMSP SSM/I-SSMIS, Version 3.Boulder, Colorado USA. NASA National Snow and Ice Data Center Distributed Active Archive Center. https://doi.org/10.5067/7Q8HCCWS4I0R.

Cota, G.F., Pomeroy, L.R., Harrison, W.G., Jones, E.P., Peters, F., Sheldon, Jr, W.M., Weingartner, T.R., 1996. Nutrients, primary production and microbial heterotrophy in the southeastern Chukchi Sea: Arctic summer nutrient depletion and heterotrophy. Mar. Ecol. Prog. Ser. 135, 247–258. https://doi.org/10.3354/meps135247

Dai, A., Luo, D., Song, M., Liu, J., 2019. Arctic amplification is caused by sea-ice loss under increasing CO_2. Nat. Commun. 10(1), 121. https://doi.org/10.1038/s41467-018-07954-9

Danielson, S.L., Ahkinga, O., Ashjian, C., Basyuk, E., Cooper, L.W., Eisner, L., Farley, E., Iken, K.B., Grebmeier, J.M., Juranek, L., Khen, G., Jayne, S., Kikuchi, T., Ladd, C., Lu, K., McCabe, R., Moore, G.W.K., Nishino, S., Okkonen, S.R., Ozenna, F., Pickart, R.S., Polyakov, I., Stabeno, P.J., Wood, K., Williams, W.J., Woodgate, R.A., Weingartner, T.J., this issue. Manifestation and consequences of warming and altered heat fluxes over the Bering and Chukchi Sea continental shelves. Deep-Sea Res. Part II-Top. Stud. Oceanogr.

Danielson, S.L., Eisner, L., Ladd, C., Mordy, C., Sousa, L., Weingartner, T.J., 2017. A comparison between late summer 2012 and 2013 water masses, macronutrients, and phytoplankton standing crops in the northern Bering and Chukchi Seas. Deep-Sea Res. Part II-Top. Stud. Oceanogr. 135, 7–26. https://doi.org/10.1016/j.dsr2.2016.05.024

Danielson, S.L., Weingartner, T.J., Hedstrom, K.S., Aagaard, K., Woodgate, R., Curchitser, E., Stabeno, P.J., 2014. Coupled wind-forced controls of the Bering–Chukchi shelf circulation and the Bering Strait throughflow: Ekman transport, continental shelf waves, and variations of the Pacific–Arctic sea surface height gradient. Prog. Oceanogr. 125, 40–61. https://doi.org/10.1016/j.pocean.2014.04.006

Frey, K.E., Moore, G.W.K., Cooper, L.W., Grebmeier, J.M., 2015. Divergent patterns of recent sea ice cover across the Bering, Chukchi, and Beaufort seas of the Pacific Arctic Region. Prog. Oceanogr. 136, 32–49. https://doi.org/10.1016/j.pocean.2015.05.009

Gong, D., Pickart, R.S., 2015. Summertime circulation in the eastern Chukchi Sea. Deep-Sea Res. Part II-Top. Stud. Oceanogr. 118, 18–31. https://doi.org/10.1016/j.dsr2.2015.02.006

Gordon, L.I., Jennings, J.C., Ross, A.A., Krest, J.M., 1994. A suggested protocol for continuous flow analysis of seawater nutrients (phosphate, nitrate, nitrite, and silicic acid) in the WOCE Hydrographic Program and the Joint Global Ocean Fluxes Study. WHP Office Report 91(1).

Hansell, D.A., Whitledge, T.E., Goering, J.J., 1993. Patterns of nitrate utilization and new production over the Bering-Chukchi shelf. Cont. Shelf Res. 13(5-6), 601–627. https://doi.org/10.1016/0278-4343(93)90096-G

Hauri, C., Danielson, S., McDonnell, A.M.P., Hopcroft, R.R., Winsor, P., Shipton, P., Lalande, C., Stafford, K.M., Horne, J.K., Cooper, L.W., Grebmeier, J.M., Mahoney, A., Maisch, K., McCammon, M., Statscewich, H., Sybrandy, A., Weingartner, T., 2018. From sea ice to seals: A moored marine ecosystem observatory in the Arctic. Ocean Sci. 14(6), 1423–1433. https://doi.org/10.5194/os-14-1423-2018

Hill, V., Ardyna, M., Lee, S.H., Varela, D.E., 2018. Decadal trends in phytoplankton production in the Pacific Arctic Region from 1950 to 2012. Deep-Sea Res. Part II-Top. Stud. Oceanogr. 152, 82–94. https://doi.org/10.1016/j.dsr2.2016.12.015

Hill, V., Cota, G., 2005. Spatial patterns of primary production on the shelf, slope and basin of the Western Arctic in 2002. Deep-Sea Res. Part II-Top. Stud. Oceanogr. 52(24-26), 3344–3354. https://doi.org/10.1016/j.dsr2.2005.10.001

Hill, V.J., Zimmerman, R.C., 2010. Estimates of primary production by remote sensing in the Arctic Ocean: assessment of accuracy with passive and active sensors. Deep-Sea Res. Part I-Oceanogr. Res. Pap. 57(10), 1243–1254. https://doi.org/10.1016/j.dsr.2010.06.011

Ladd, C., Mordy, C.W., Salo, S.A., Stabeno, P.J., 2016. Winter water properties and the Chukchi Polynya. J. Geophys. Res.-Oceans 121(8), 5516–5534. https://doi.org/10.1002/2016JC011918

Lewis, K.M., Arntsen, A.E., Coupel, P., Joy-Warren, H., Lowry, K.E., Matsuoka, A., Mills, M.M., van Dijken, G.L., Selz, V., Arrigo, K.R., 2019. Photoacclimation of Arctic Ocean phytoplankton to shifting light and nutrient limitation. Limnol. Oceanogr. 64(1), 284–301. https://doi.org/10.1002/lno.11039

Li, M., Pickart, R.S, Spall, M.A., Weingartner, T.J., Lin, P., Moore, G.W.K., Qi, Y., 2019. Circulation of the Chukchi Sea shelfbreak and slope from moored timeseries. Prog. Oceanogr. 172, 14–33. https://doi.org/10.1016/j.pocean.2019.01.002

Lin, P., Pickart, R.S., McRaven, L.T., Arrigo, K.R., Bahr, F., Lowry, K.E., Stockwell, D.A., Mordy, C.W., 2019. Water mass evolution and circulation of the northeastern Chukchi Sea in summer: Implications for nutrient distributions. J. Geophys. Res.-Oceans 124(7), 4416–4432. https://doi.org/10.1029/2019JC015185

Linders, J., Pickart, R.S., Björk, G., Moore, G.W.K., 2017. On the nature and origin of water masses in Herald Canyon, Chukchi Sea: Synoptic surveys in summer 2004, 2008, and 2009. Prog. Oceanogr. 159, 99–114. https://doi.org/10.1016/j.pocean.2017.09.005

Lowry, K.E., Pickart, R.S., Mills, M.M., Brown, Z.W., van Dijken, G.L., Bates, N.R., Arrigo, K.R., 2015. The influence of winter water on phytoplankton blooms in the Chukchi Sea. Deep-Sea Res. Part II-Top. Stud. Oceanogr. 118, 53–72. https://doi.org/10.1016/j.dsr2.2015.06.006

Macdonald, R.W., Anderson, L.G., Christensen, J.P., Miller, L.A., Semiletov, I.P., Stein, R., 2010. The Arctic Ocean, in: Liu, K.-K., Atkinson, L., Quiñones, R., Talaue-McManus, L. (Eds.), Carbon and Nutrient Fluxes in Continental Margins: A Global Synthesis. Springer Berlin Heidelberg, pp. 291–303.

Mesinger, F., DiMego, G., Kalnay, E., Mitchell, K., Shafran, P.C., Ebisuzaki, W., Jović, D., Woollen, J., Rogers, E., Berbery, E.H., Ek, M.B., Fan, Y., Grumbine, R., Higgins, W., Li, H., Lin, Y., Manikin, G., Parrish, D., Shi, W., 2006. North American Regional Reanalysis. Bull. Am. Meteorol. Soc. 87(3), 343–360. https://doi.org/10.1175/BAMS-87-3-343

Mills, M.M., Brown, Z.W., Lowry, K.E., van Dijken, G.L., Becker, S., Pal, S., Benitez-Nelson, C.R., Downer, M.M., Strong, A.L., Swift, J.H., Pickart, R.S., Arrigo, K.R., 2015. Impacts of low phytoplankton NO_3^-:PO_4^{3-} utilization ratios over the Chukchi Shelf, Arctic Ocean.

Deep-Sea Res. Part II-Top. Stud. Oceanogr. 118, 105–121. https://doi.org/10.1016/j.dsr2.2015.02.007

Mordy, C.W., Stabeno, P.J., Kachel, N.B., Kachel, D., Ladd, C., Zimmermann, M., Hermann, A.J., Coyle, K.O., Doyle, M., 2019. Patterns of flow in the canyons of the northern Gulf of Alaska. Deep-Sea Res. Part II-Top. Stud. Oceanogr. 165, 203–220. https://doi.org/10.1016/j.dsr2.2019.03.009

Mordy, C.W., Stabeno, P.J., Ladd, C., Zeeman, S.I., Wisegarver, D.P., Hunt Jr., G.L., 2005. Nutrients and primary production along the eastern Aleutian Island Archipelago. Fish. Oceanogr. 14, 55–76. https://doi.org/10.1111/j.1365-2419.2005.00364.x

Neeley, A.R., Harris, L.A., Frey, K.E., 2018. Unraveling phytoplankton community dynamics in the northern Chukchi Sea under sea-ice-covered and sea-ice-free conditions. Geophys. Res. Lett. 45(15), 7663–7671. https://doi.org/10.1029/2018GL077684

Nishino, S., Kikuchi, T., Fujiwara, A., Hirawake, T., Aoyama, M., 2016. Water mass characteristics and their temporal changes in a biological hotspot in the southern Chukchi Sea. Biogeosciences 13(8), 2563–2578. https://doi.org/10.5194/bg-13-2563-2016

Overland, J.E., Wang, M., 2018. Arctic-midlatitude weather linkages in North America. Polar Sci. 16, 1–9. https://doi.org/10.1016/j.polar.2018.02.001

Peralta-Ferriz, C., Woodgate, R.A., 2017. The dominant role of the East Siberian Sea in driving the oceanic flow through the Bering Strait—Conclusions from GRACE ocean mass satellite data and in situ mooring observations between 2002 and 2016. Geophys. Res. Lett. 44(22), 11472–11481. https://doi.org/10.1002/2017GL075179

Roach, A.T., Aagaard, K., Pease, C.H., Salo, S.A., Weingartner, T., Pavlov, V., Kulakov, M., 1995. Direct measurements of transport and water properties through the Bering Strait. J. Geophys. Res.-Oceans 100(C9), 18443–18457. https://doi.org/10.1029/95JC01673

Rolph, R.J., Mahoney, A.R., Walsh, J., Loring, P.A., 2018. Impacts of a lengthening open water season on Alaskan coastal communities: deriving locally relevant indices from large-scale datasets and community observations. Cryosphere 12(5), 1779–1790. https://doi.org/10.5194/tc-12-1779-2018

Sakshaug, E., 2004. Primary and secondary production in the Arctic Seas, in: Stein, R., MacDonald, R.W. (Eds.), The Organic Carbon Cycle in the Arctic Ocean. Springer Publishing Company, Berlin, pp. 57–81.

Sambrotto, R.N., Goering, J.J., McRoy, C.P., 1984. Large yearly production of phytoplankton in the western Bering Strait. Science 225(4667), 1147–1150. https://doi.org/10.1126/science.225.4667.1147

Schumacher, J.D., Stabeno, P.J., Roach, A.T., 1989. Volume transport in the Alaska Coastal Current. Cont. Shelf Res. 9(12), 1071–1083. https://doi.org/10.1016/0278-4343(89)90059-9

Screen, J.A. Simmonds, I., 2010. The central role of diminishing sea-ice in recent Arctic temperature amplification. Nature 464, 1334–1337. https://doi.org/10.1038/nature09051

Selz, V., Laney, S., Arnsten, A.E., Lewis, K.M., Lowry, K.E., Joy-Warren, H.L., Mills, M.M., van Dijken, G.L., Arrigo, K.R., 2018. Ice algal communities in the Chukchi and Beaufort Seas in spring and early summer: Composition, distribution, and coupling with phytoplankton assemblages. Limnol. Oceanogr. 63(3), 1109–1133. https://doi.org/10.1002/lno.10757

Serreze, M.C., Barrett, A.P., Stroeve, J.C., Kindig, D.N., Holland, M.M., 2009. The emergence of surface-based Arctic amplification. Cryosphere 3, 11–19. https://doi.org/10.5194/tc-3-11-2009

Serreze, M.C., Stroeve, J., Barrett, A.P., Boisvert, L.N., 2016. Summer atmospheric circulation anomalies over the Arctic Ocean and their influences on September sea ice extent: A cautionary tale. J. Geophys. Res.-Atmos. 121(19), 11463–11485. https://doi.org/10.1002/2016JD025161

Spall, M.A., 2007. Circulation and water mass transformation in a model of the Chukchi Sea. J. Geophys. Res.-Oceans 112(C5), C05025. https://doi.org/10.1029/2005JC003364

Springer, A.M., McRoy, C.P., 1993. The paradox of pelagic food webs in the northern Bering Sea—III. Patterns of primary production. Cont. Shelf Res. 13(5–6), 575–599. https://doi.org/10.1016/0278-4343(93)90095-F

Stabeno, P.J., 2019. The Eastern Bering Sea: Declining ice, warming seas, and a changing ecosystem, in *State of the Climate in 2018*. Bull. Am. Meteorol. Soc. 100(9), S148–S149.

Stabeno, P.J., Bell, S.W., 2019. Extreme conditions in the Bering Sea (2017-2018): Record breaking low sea-ice extent. Geophys. Res. Lett. 46, 8952–8959. https://doi.org/10.1029/2019GL083816

Stabeno, P.J., Bell, S.W., Bond, N.A., Kimmel, D.G., Mordy, C.W., Sullivan, M.E., 2018a. Distributed Biological Observatory Region 1: Physics, chemistry and plankton in the northern Bering Sea. Deep-Sea Res. Part II- Top. Stud. Oceanogr. 162, 8–21. https://doi.org/10.1016/j.dsr2.2018.11.006

Stabeno, P.J., Bell, S., Cheng, W., Danielson, S., Kachel, N.B., Mordy, C.W., 2016a. Long-term observations of Alaska Coastal Current in the northern Gulf of Alaska. Deep-Sea Res. Part II-Top. Stud. Oceanogr. 132, 24–40. https://doi.org/10.1016/j.dsr2.2015.12.016

Stabeno, P.J., Danielson, S.L., Kachel, D.G., Kachel, N.B., Mordy, C.W., 2016b. Currents and transport on the eastern Bering Sea shelf: An integration of over 20 years of data. Deep-Sea Res. Part II-Top. Stud. Oceanogr. 134, 13–29. https://doi.org/10.1016/j.dsr2.2016.05.010

Stabeno, P.J., Hristova, H.G., 2014. Observations of the Alaskan Stream near Samalga Pass and its connection to the Bering Sea: 2001– 2004. Deep-Sea Res. Part I-Oceanogr. Res. Pap. 88, 30–46. https://doi.org/10.1016/j.dsr.2014.03.002

Stabeno, P., Kachel, N., Ladd, C., Woodgate, R., 2018b. Flow patterns in the eastern Chukchi Sea: 2010–2015. J. Geophys. Res. 123(2), 1177–1195. https://doi.org/10.1002/2017JC013135

Stabeno, P., Mordy, C.W., Sigler, M., Seasonal patterns of primary production at the seafloor in the eastern Chukchi Sea based upon *in-situ* chlorophyll fluorescence measurements, 2010-2018. Deep-Sea Res. Part II- Top. Stud. Oceanogr. (this issue)

Stabeno, P J., Reed, R.K., Schumacher, J.D., 1995. The Alaska Coastal Current: Continuity of transport and forcing. J. Geophys. Res.-Oceans 100(C2), 2477–2485. https://doi.org/10.1029/94JC02842

Steele, M., Ermold, W., Zhang, J., 2008. Arctic Ocean surface warming trends over the past 100 years. Geophys. Res. Lett. 35(2), L02614. https://doi.org/10.1029/2007GL031651

Stein, R., Macdonald, R.W., 2004. The Organic Carbon Cycle in the Arctic Ocean. Springer Publishing Company, Berlin. https://doi.org/10.1007/978-3-642-18912-8

Stigebrandt, A., 1984. The North Pacific: A global-scale estuary. J. Phys. Oceanogr. 14(2), 464–470.

Tachibana, Y., Komatsu, K.K., Alexeev, V.A., Cai, L., Ando, Y., 2019. Warm hole in Pacific Arctic sea ice cover forced mid-latitude Northern Hemisphere cooling during winter 2017–18. Sci. Rep. 9(1), 5567. https://doi.org/10.1038/s41598-019-41682-4

Torres-Valdés, S., Tsubouchi, T., Bacon, S., Naveira-Garabato, A.C., Sanders, R., McLaughlin, F.A., .Petrie, B., Kattner, G., Azetsu-Scott, K., Whitledge, T.E., 2013. Export of nutrients from the Arctic Ocean. J. Geophys. Res.-Oceans 118(4), 1625–1644. https://doi.org/10.1002/jgrc.20063

Tremblay, G., Belzile, C., Gosselin, M., Poulin, M., Roy, S., Tremblay, J.-É., 2009. Late summer phytoplankton distribution along a 3500 km transect in Canadian Arctic waters: Strong numerical dominance by picoeukaryotes. Aquat. Microb. Ecol. 54(1), 55–70. https://doi.org/10.3354/ame01257

Tremblay, J.-É., Michel, C., Hobson, K.A., Gosselin, M., Price, N.M., 2006. Bloom dynamics in early opening waters of the Arctic Ocean. Limnol. Oceanogr. 51(2), 900–912. https://doi.org/10.4319/lo.2006.51.2.0900

Walsh, J.J., McRoy, C.P., Coachman, L.K., Goering, J.J., Nihoul, J.J., Whitledge, T.E., Blackburn, T.H., Parker, P.L., Wirick, C.D., Shuert, P.G., Grebmeier, J.M., Springer, A.M., Tripp, R.D., Hansell, D.A., Djenidi, S., Deleersnijder, E., Henriksen, K., Lund, B.A., Andersen, P., Müller-Karger, F.E., Dean, K., 1989. Carbon and nitrogen cycling within the Bering/Chukchi Seas: Source regions for organic matter effecting AOU demands of the Arctic Ocean. Prog. Oceanogr. 22(4), 277–359. https://doi.org/10.1016/0079-6611(89)90006-2

Wang, M., Overland, J.E., 2015. Projected future duration of the sea-ice-free season in the Alaskan Arctic. Prog. Oceanogr. 136, 50–59. https://doi.org/10.1016/j.pocean.2015.01.001

Wang, M., Yang, Q., Overland, J.E., Stabeno, P., 2018. Sea-ice cover timing in the Pacific Arctic: The present and projections to mid-century by selected CMIP5 models. Deep-Sea Res. Part II-Top. Stud. Oceanogr. 152, 22–34. https://doi.org/10.1016/j.dsr2.2017.11.017

Weingartner, T.J., Cavalieri, D.J., Aagaard, K., Sasaki, Y., 1998. Circulation, dense water formation, and outflow on the northeast Chukchi shelf. J. Geophys. Res.-Oceans 103(C4), 7647–7661. https://doi.org/10.1029/98JC00374

Weingartner, T.J., Danielson, S., Sasaki, Y., Pavlov, V., Kulakov, M., 1999. The Siberian Coastal Current: A wind- and buoyancy-forced Arctic coastal current. J. Geophys. Res.-Oceans 104(C12), 29697–29713. https://doi.org/10.1029/1999JC900161

Wood, K.R., Bond, N.A., Danielson, S.L., Overland, J.E., Salo, S.A., Stabeno, P.J., Whitefield, J., 2015. A decade of environmental change in the Pacific Arctic region. Prog. Oceanogr. 136, 12–31. https://doi.org/10.1016/j.pocean.2015.05.005

Wood, K.R., Jayne, S.R., Mordy, C.W., Bond, N., Overland, J.E., Ladd, C., Stabeno, P.J., Ekholm, A.K., Robbins, P.E., Schreck, M.-B., Heim, R., Intieri, J., 2018. Results of the first Arctic Heat Open Science Experiment. Bull. Am. Meteorol. Soc. 99(3), 513–520. https://doi.org/10.1175/BAMS-D-16-0323.1

Woodgate, R.A., 2018. Increases in the Pacific inflow to the Arctic from 1990 to 2015, and insights into seasonal trends and driving mechanisms from year-round Bering Strait mooring data. Prog. Oceanogr. 160, 124–154. https://doi.org/10.1016/j.pocean.2017.12.007

Woodgate, R.A., Aagaard, K., Weingartner, T.J., 2005. A year in the physical oceanography of the Chukchi Sea: Moored measurements from autumn 1990–1991. Deep-Sea Res. Part II-Top. Stud. Oceanogr. 52(24-26), 3116–3149. https://doi.org/10.1016/j.dsr2.2005.10.016

Woodgate, R.A., Weingartner, T.J., Lindsay, R., 2012. Observed increases in Bering Strait oceanic fluxes from the Pacific to the Arctic from 2001 to 2011 and their impacts on the Arctic Ocean water column. Geophys. Res. Lett. 39(24), L24603. https://doi.org/10.1029/2012GL054092

Zhang, J., 2005. Warming of the arctic ice-ocean system is faster than the global average since the 1960s. Geophys. Res. Lett. 32(19), L19602. https://doi.org/10.1029/2005GL024216

Tables

Table 1. The locations and bottom depths of the Icy Cape moorings.

Mooring	Latitude (°N)	Longitude (°W)	Depth (m)
C1	70.835	163.119	44
C2	71.222	164.250	45
C3	71.825	165.975	45

Table 2. Temperature and salinity bounds for water masses observed in this study. The classification scheme follows Danielson et al. (2017), modified by Ladd et al. (2016) for identification of water influenced by brine exclusion.

Water Mass	Temperature (°C)	Salinity
Winter Water	$-2 < T < 0$	$30.0 \leq S \leq 33.6$
Summer Water	$0 \leq T < 7$	$30.0 \leq S \leq 33.6$
Atlantic Water	$-1 \leq T < 1$	$33.6 < S < 35.0$
Brine Exclusion	$-2 < T < -1$	$33.6 < S < 35.0$

Table 3. Mean and standard deviation of nitrate and dissolved inorganic nitrogen (DIN) concentrations in bottom water on the northern Bering Sea in spring (March–May) and summer/fall (July–October). Data are from 5 cruises in spring and 23 cruises in summer/fall spanning 2004 – 2018. Stations were located between 61.5° and 63.6°N and 55–90 m water depth, and samples were from the deepest Niskin bottle providing that it was < 12 m from the bottom. Cruises in spring were conducted in ice-covered waters in 2007–2010 as part of the Bering Sea Ecosystem Study (BEST), and in ice-free waters in May 2018 during the NOAA-PMEL spring mooring cruise.

	Nitrate (µM)	DIN (µM)	N
March–May	13.5 ± 4.0	14.9 ± 3.6	92
July–October	10.8 ± 3.2	14.4 ± 3.5	207

Figures

Figure 1. Map of the Chukchi Sea (modified from Ladd et al., 2016) showing patterns of flow (yellow arrows) including the Siberian Coastal Current (SCC) and Alaskan Coastal Current (ACC), and the locations of the Icy Cape moorings (C1, C2, and C3) and the Icy Cape hydrographic line (green bar). The red boxes around each of the moorings denotes the boxes for determining ice concentration.

Figure 2. Annual time series of the percent areal ice cover (black), nitrate (blue), salinity (red), chlorophyll fluorescence (green), and water mass (color bar atop each panel) from six deployments at the C2 mooring spanning 2010–2012 and 2014–2018. Filled circles indicate discrete nitrate calibration points. Water types include summer water (red), winter water (blue), Atlantic water (white), and brine-influenced water (black).

Figure 3. Multi-year (2011, 2012, 2015–2018) hourly mean (a) and anomalies (b-g) of nitrate (blue) and salinity (red) at the C2 mooring in January through May for the six time series shown in Fig. 2. Note the change in scale in 2018. The mean does not include nitrate data from 20–31 May 2018, and the nitrate anomaly during this period is off-scale at -12.1 µM.

Figure 4. Nitrate-Salinity relationship at the C2 mooring from 1 January to 31 May in 2012, 2015, 2016, and 2017 (green), and 2011 (orange). Data from 2018 (red) are shown from 1 January to 20 May as the seasonal drawdown of nitrate occurred thereafter. Data from the Bering Sea (blue) include 3973 near-bottom (<12 m from bottom) samples from the shelf (< 150 m) that were collected on 53 cruises spanning March to October, 2003 to 2018.

Figure 5. Annual time series of the percent areal ice cover in 50 km × 50 km box centered on each mooring (black), nitrate (blue), salinity (red), chlorophyll fluorescence (green), and

water mass (color bar atop each panel) from deployments at the C1, C2, and C3 moorings deployed in 2016 (a-c) and 2017 (d-f). Filled circles indicate discrete nitrate calibration points. Water types include summer water (red), winter water (blue), Atlantic water (white), and brine-influenced water (black).

Figure 6. Percent ice cover (blue is open water, white is ice) on 16 December 2017 showing a polynya near the C1 mooring. The inset is the T-S diagram from 15 December 2017 to 31 January 2018 for the C1 (blue), C2 (green), and C3 (red) moorings. The warmest temperatures (-0.6°C) were observed at the C1 mooring on 18 December 2017.

Figure 7. Anomalies of nitrate (blue) and salinity (red) in January through May for time series at C1, C2, and C3 in 2017 (a-c) and 2018 (d-f) using the same mean values as in Fig. 3.

Figure 8. Three-month means of transport (Sv) across the Icy Cape line. Years in gray are periods without a corresponding time series in nitrate.

Figure 9. Black symbols are the 3-day mean nitrate concentrations on 14–16 May at the six C2 time series shown in Fig. 2 compared to the mean seasonal (January–May) transport across the Icy Cape line. Blue symbols are the maximum 3-day mean nitrate concentration after 15 May compared to the mean transport from the prior 5 months with arrows indicating the increase in nitrate after 15 May. The standard error of the mean was within the symbols. The regression slopes in these comparisons were not significant.

Figure 10. (a) Summer and fall (July–October) concentrations of dissolved inorganic nitrogen (DIN) in bottom water (< 12 m from the bottom except for samples collected at 50 m in 2011) within a 1° latitude × 2° longitude box (61.8°–62.8°N, 174°–176°W) around the M8 mooring in the northern Bering Sea. Data are from 20 individual cruises between 2005 and 2018. Error bars represent the standard error of the mean for each cruise. The

regression line is from 2005 to 2016 and has a significant slope of 0.6 µM y^{-1} ($p = 0.005$, $F = 11$) shown with the 95% confidence bands. From this regression, the predicted DIN concentration on 1 October 2013 was 14.0 ± 2.6 µM (± SE, orange data point). (b) Black symbols are the 3-day mean nitrate concentrations at the C2 mooring on 14–16 May compared to mean DIN concentrations in bottom water at the M8 from the previous summer and/or fall. Blue symbols are the maximum 3-day mean nitrate concentration at the C2 mooring after 15 May with arrows indicating the increase in nitrate after 15 May as in Fig. 9. Error bars represent the standard error of the mean, and y-error bars are within the symbols. The gray line is the 1:1 ratio. Arrigo et al. (2017) reported that mean nitrate concentrations in bottom water over the shelf in May-June 2014 was 14.0 ± 1.9 µM (orange) shown with the SE of the prediction at M8.

Figure 11. Hydrographic sections along the Icy Cape line in August 2018 of salinity (a) and nitrate (c) with contours of potential density (σ_t). Identification of water types (b) are according to Danielson et al. (2017).

Figure 12. (a) Drift track of ALAMO float 9119 from 14 September 2017 to 20 November 2017 colored by bottom salinity. The diamond indicates the location of the C2 mooring. (b) Vertical profile of salinity from ALAMO float 9119 during this period. (c) Time series of nitrate (blue) and salinity (red) from the C2 mooring along with bottom salinity (yellow/green) from ALAMO float 9119. The arrows in (b) and (c) indicate the nearest approach of the float to the C2 mooring.

Figure 13. Monthly mean wind (red) and transport (a) and nitrate flux (b) across the Icy Cape line from November through May for the six mooring deployments. Transport was calculated using currents from the C1, C2, and C3 moorings, and was combined with

nitrate at C2 for determination of the nitrate flux with the assumption that the water column was well mixed during this period. In May 2018, nitrate was averaged from 1-20 May. Positive transport and nitrate flux are to the northeast, and winds are relative to north. In (b), the mean nitrate flux from November-April is shown above the x-axis, and the May nitrate flux appears above each column in May.

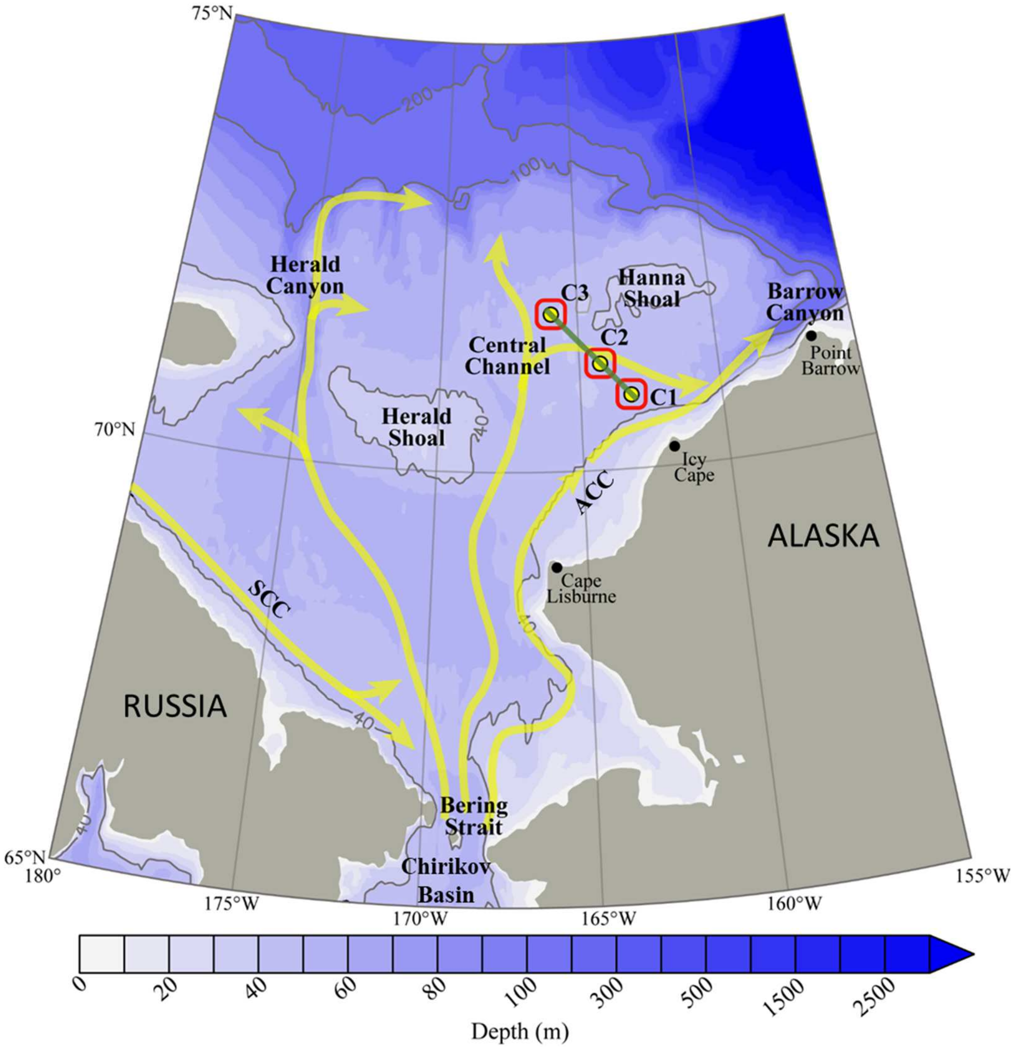
75°N
200
100
Herald
Canyon
Hanna
Shoal
Barrow
Canyon
C3
C2
C1
Central
Channel
Point
Barrow
Herald
Shoal
70°N
40
Icy
Cape
ACC
ALASKA
Cape
Lisburne
SCC
RUSSIA
Bering
Strait
Chirikov
Basin
65°N
180°
175°W
170°W
165°W
160°W
155°W
0
20
40
60
80
100
300
500
1500
2500
Depth (m)

Figure 1

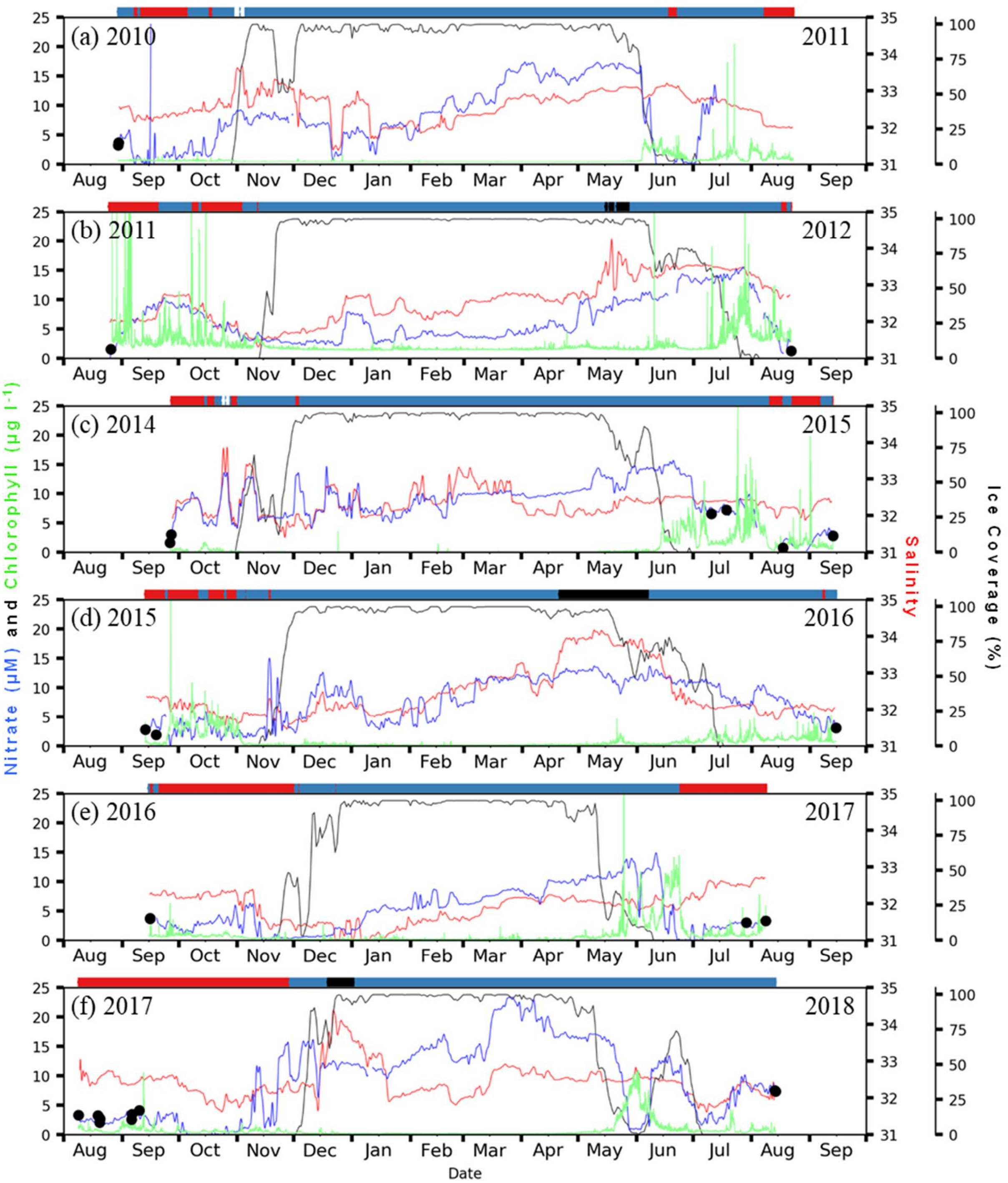
(a) 2010
2011
(b) 2011
2012
(c) 2014
2015
(d) 2015
2016
(e) 2016
2017
(f) 2017
2018
Aug Sep Oct Nov Dec Jan Feb Mar Apr May Jun Jul Aug Sep
Date
Nitrate (μM) and Chlorophyll (μg l⁻¹)
Salinity
Ice Coverage (%)

Figure 2

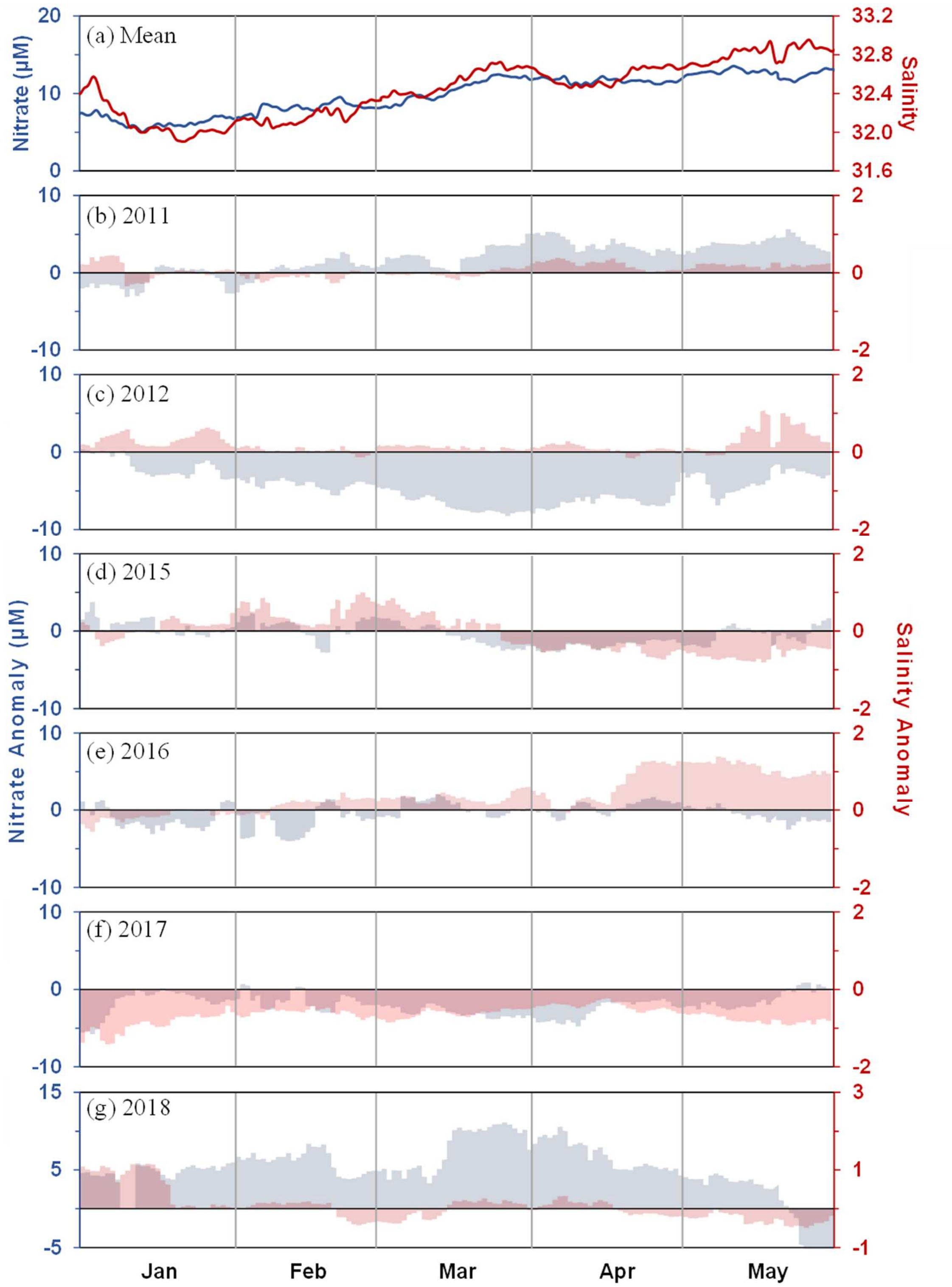
(a) Mean
(b) 2011
(c) 2012
(d) 2015
(e) 2016
(f) 2017
(g) 2018
Nitrate (µM)
Salinity
Nitrate Anomaly (µM)
Salinity Anomaly
Jan
Feb
Mar
Apr
May

Figure 3

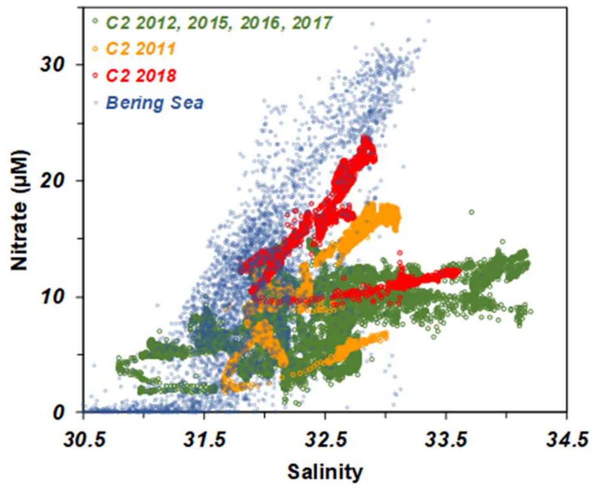
C2 2012, 2015, 2016, 2017
C2 2011
C2 2018
Bering Sea
Nitrate (µM)
30
20
10
0
30.5
31.5
32.5
33.5
34.5
Salinity

Figure 4

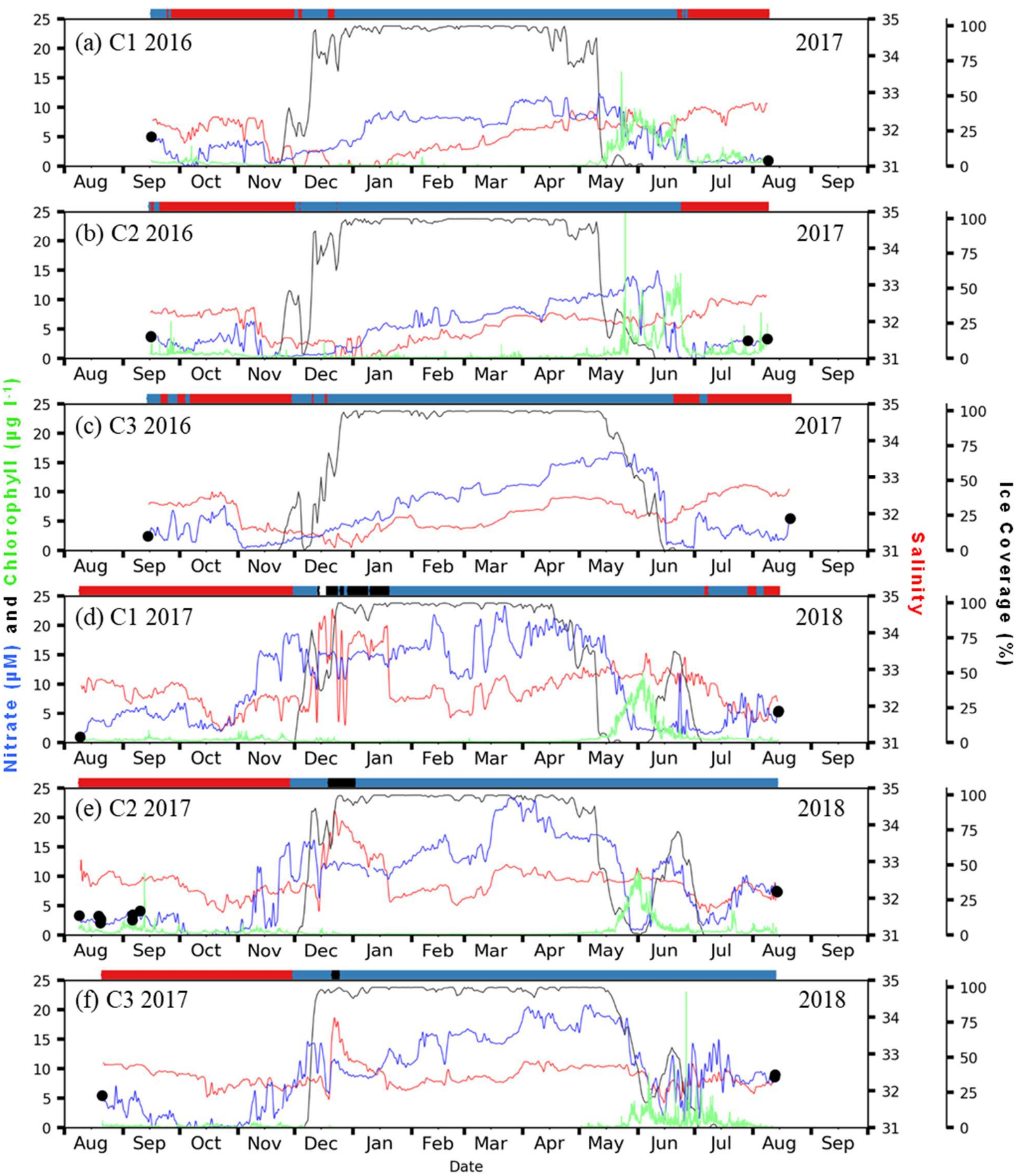

955

956 Figure 5

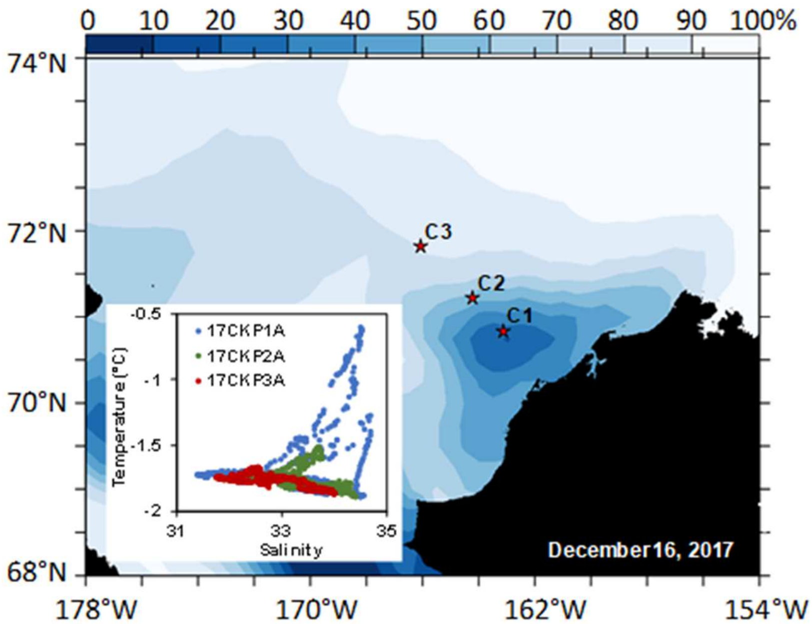
0
10
20
30
40
50
60
70
80
90
100%
74°N
72°N
70°N
68°N
178°W
170°W
162°W
154°W
C3
C2
C1
-0.5
-1
-1.5
-2
Temperature (°C)
17CKP1A
17CKP2A
17CKP3A
31
33
35
Salinity
December 16, 2017

Figure 6

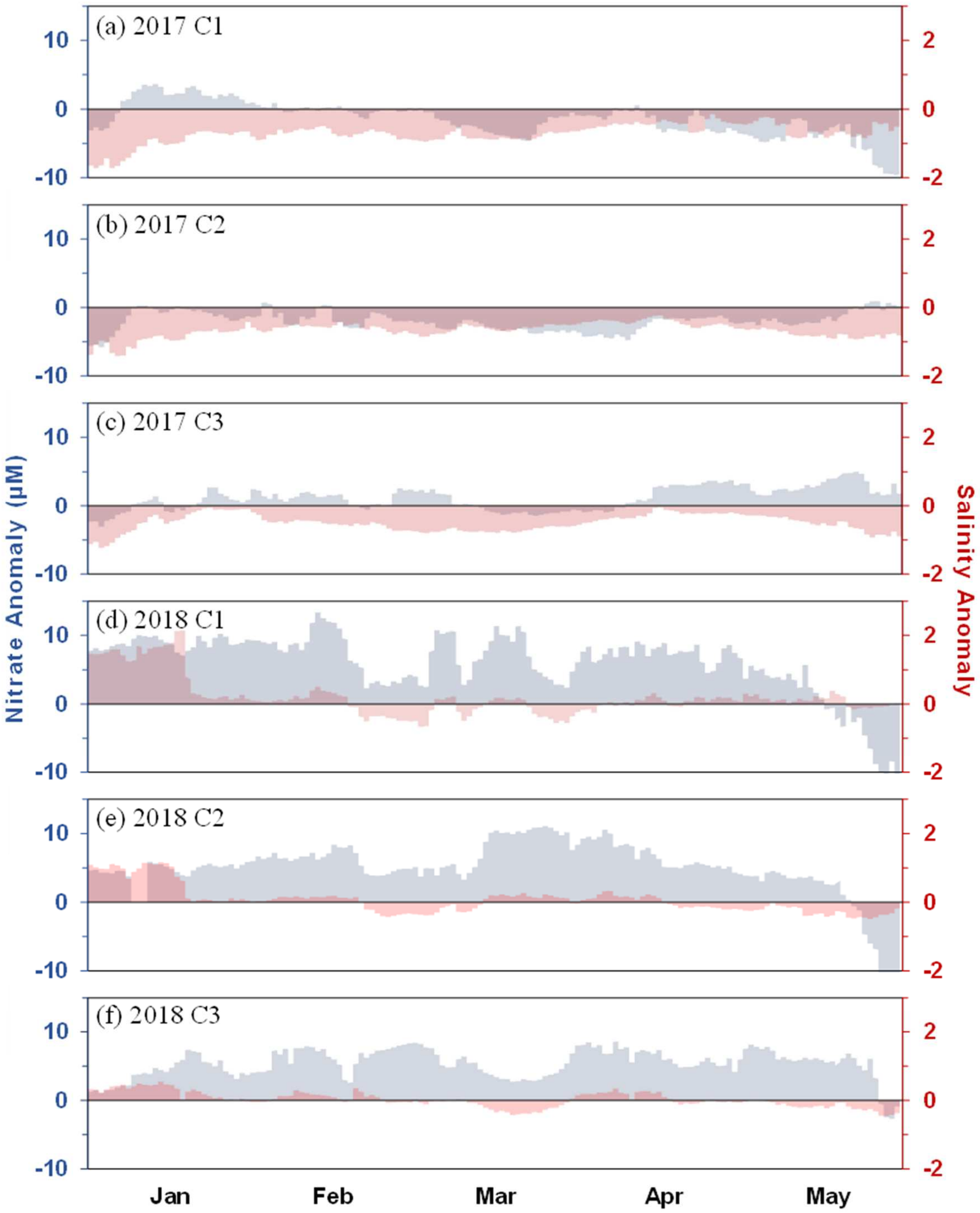
(a) 2017 C1
(b) 2017 C2
(c) 2017 C3
(d) 2018 C1
(e) 2018 C2
(f) 2018 C3
Nitrate Anomaly (μM)
Salinity Anomaly
10
0
-10
2
0
-2
Jan
Feb
Mar
Apr
May

Figure 7

	SON	OND	NDJ	DJF	JFM	FMA	MAM
2017 – 2018	1.1	1.0	0.8	0.7	0.9	0.9	0.5
2016 – 2017	0.5	0.5	0.6	0.5	0.6	0.4	0.5
2015 – 2016	0.5	0.0	0.0	-0.1	0.1	0.1	0.2
2014 – 2015	0.4	0.1	0.1	0.1	0.3	0.2	0.3
2013 – 2014	0.5	0.5	0.1	-0.1	-0.1	0.2	0.5
2012 – 2013	0.4	0.4	0.1	-0.2	-0.2	0.0	0.3
2011 – 2012	0.1	0.0	0.0	0.0	0.1	0.0	0.1
2010 – 2011	0.2	-0.1	0.2	0.6	0.9	0.6	0.4

Scale

-1 -0.5 0.0 0.5 1 (Sv)

Figure 8

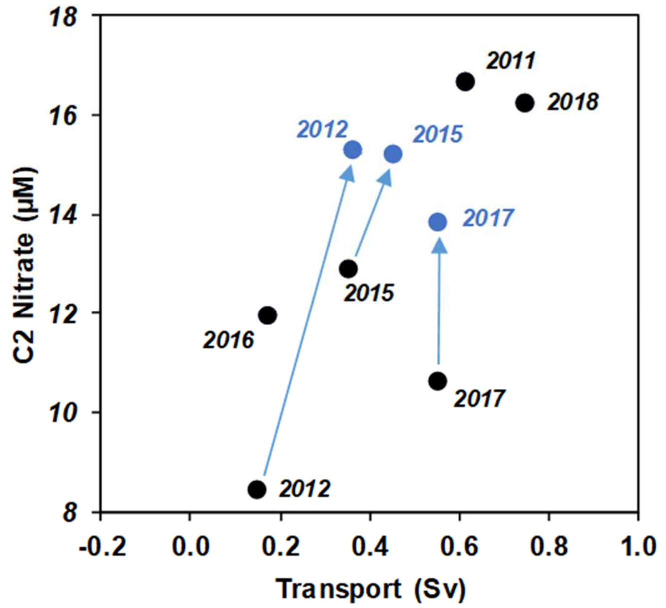

C2 Nitrate (µM)
Transport (Sv)
18
16
14
12
10
8
-0.2
0.0
0.2
0.4
0.6
0.8
1.0
2011
2018
2012
2015
2017
2015
2016
2017
2012

Figure 9

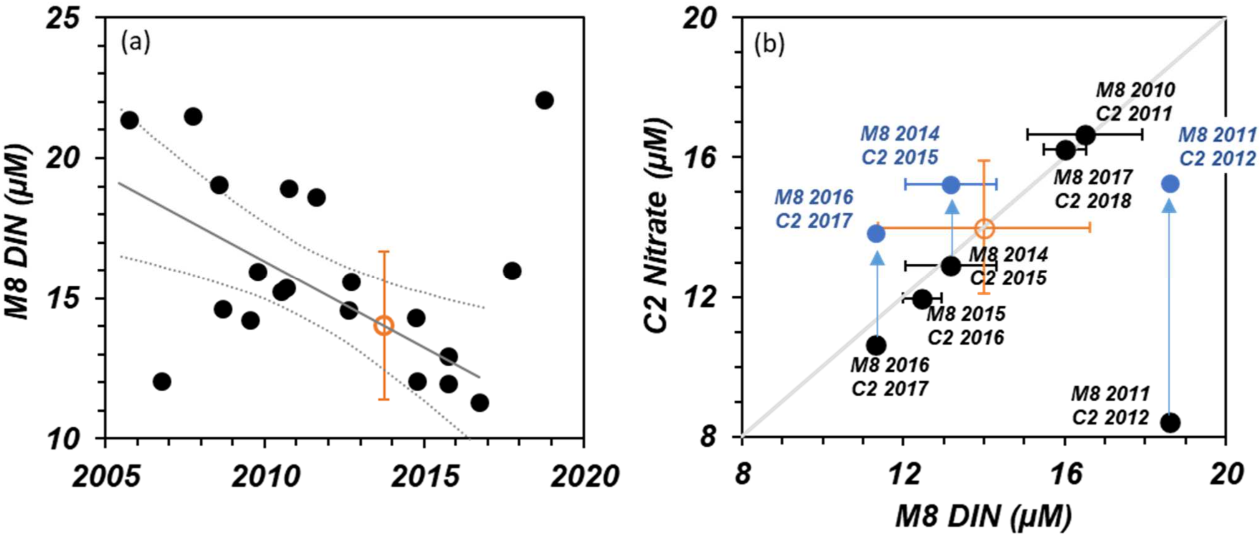
(a)
25
20
15
10
M8 DIN (µM)
2005
2010
2015
2020
(b)
20
16
12
8
C2 Nitrate (µM)
8
12
16
20
M8 DIN (µM)
M8 2010
C2 2011
M8 2014
C2 2015
M8 2011
C2 2012
M8 2017
C2 2018
M8 2016
C2 2017
M8 2014
C2 2015
M8 2015
C2 2016
M8 2016
C2 2017
M8 2011
C2 2012

Figure 10

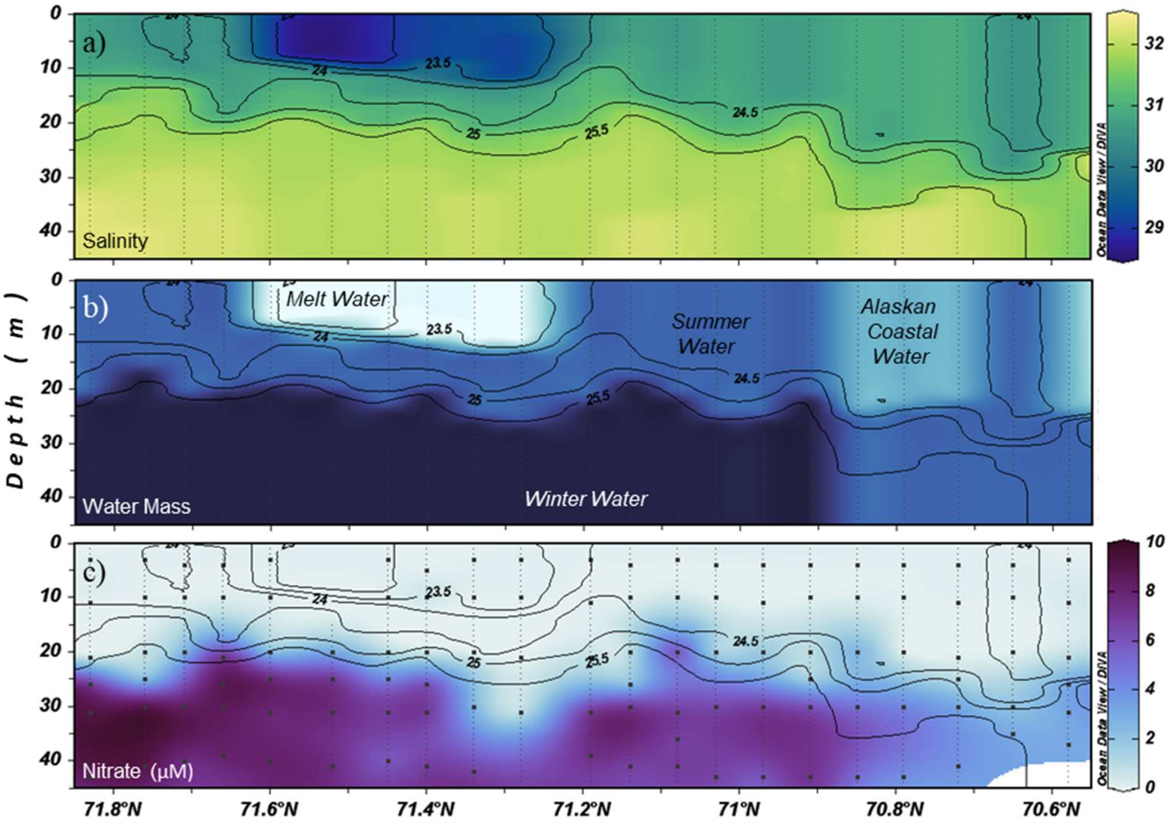
a)
Salinity
b)
Melt Water
Summer Water
Alaskan Coastal Water
Winter Water
Water Mass
c)
Nitrate (µM)
Depth (m)
0
10
20
30
40
71.8°N
71.6°N
71.4°N
71.2°N
71°N
70.8°N
70.6°N
23.5
24
24.5
25
25.5
Ocean Data View / DIVA

Figure 11

Figure 12

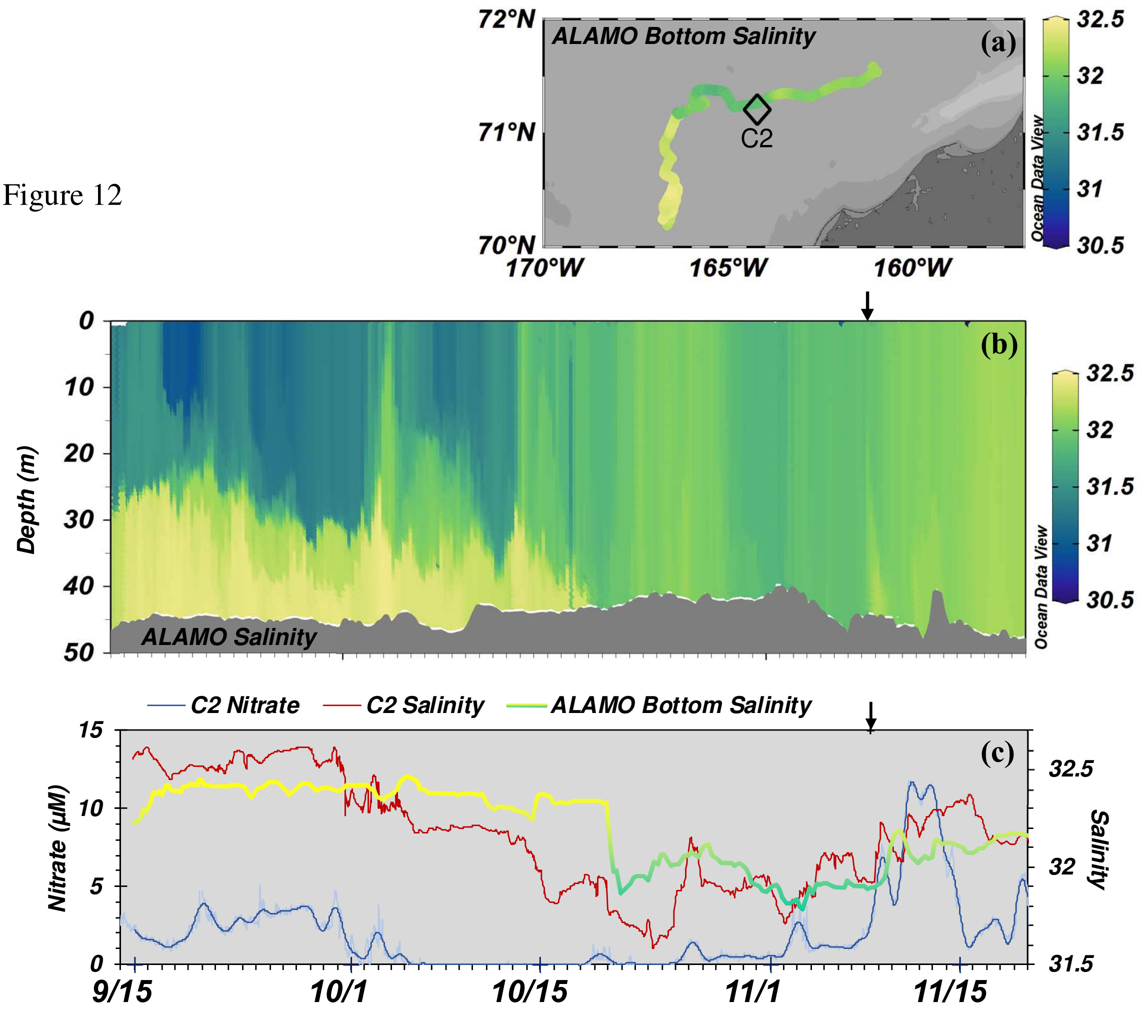
ALAMO Bottom Salinity
(a)
C2
72°N
71°N
70°N
170°W
165°W
160°W
32.5
32
31.5
31
30.5
Ocean Data View
(b)
Depth (m)
0
10
20
30
40
50
ALAMO Salinity
32.5
32
31.5
31
30.5
Ocean Data View
C2 Nitrate
C2 Salinity
ALAMO Bottom Salinity
(c)
Nitrate (μM)
15
10
5
0
Salinity
32.5
32
31.5
9/15
10/1
10/15
11/1
11/15

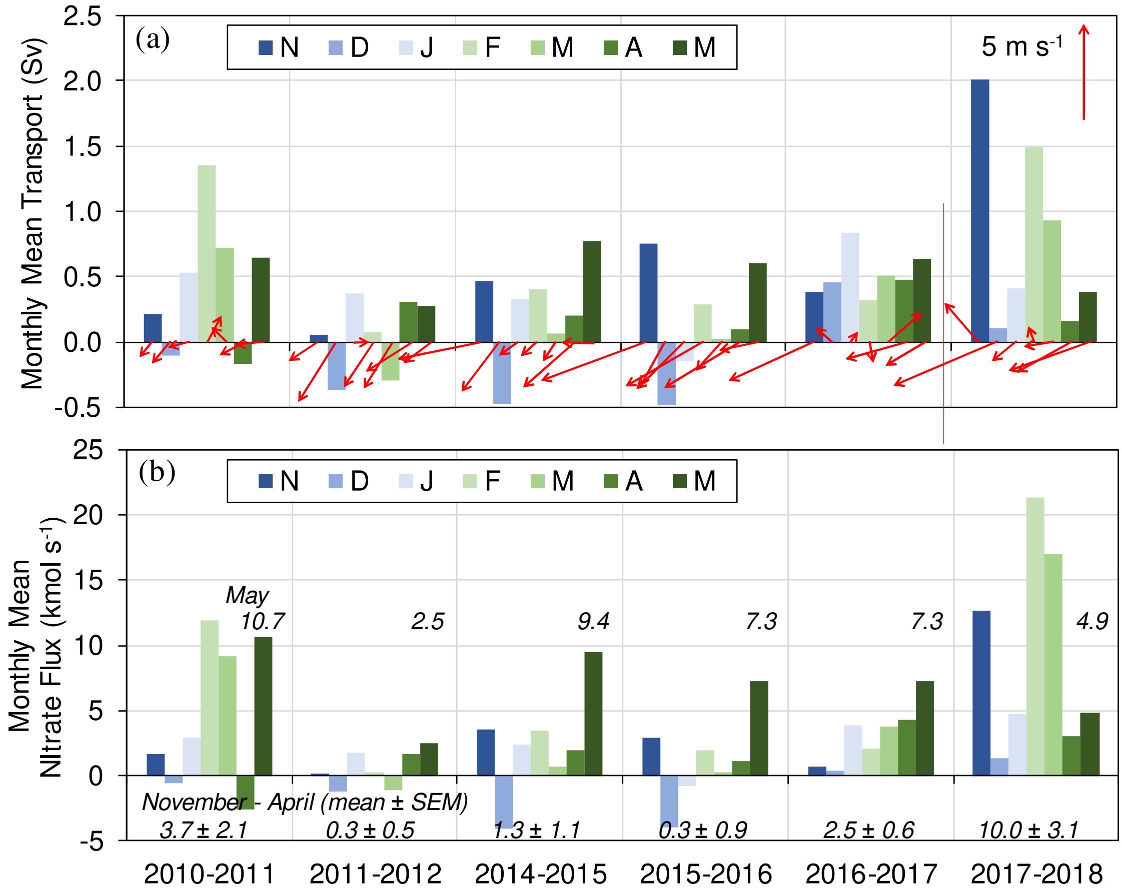
(a)
N D J F M A M
5 m s-1
Monthly Mean Transport (Sv)
2.5
2.0
1.5
1.0
0.5
0.0
-0.5
(b)
N D J F M A M
Monthly Mean
NItrate Flux (kmol s-1)
25
20
15
10
5
0
-5
May
10.7
2.5
9.4
7.3
7.3
4.9
November - April (mean ± SEM)
3.7 ± 2.1
0.3 ± 0.5
1.3 ± 1.1
0.3 ± 0.9
2.5 ± 0.6
10.0 ± 3.1
2010-2011
2011-2012
2014-2015
2015-2016
2016-2017
2017-2018

Figure 13

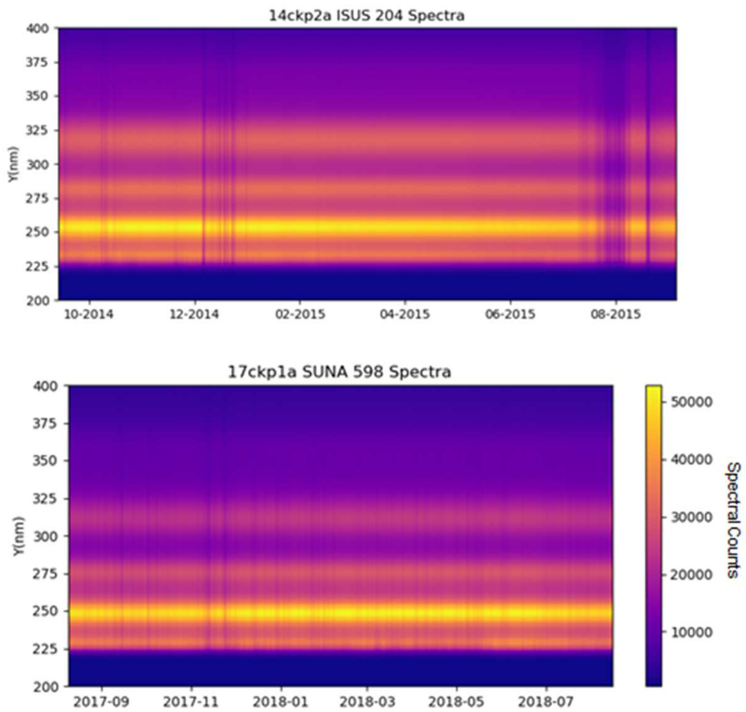

Fig. S1. Comparison of spectral time series plots from the ISUS (top) and SUNA (bottom) with wavelength on the y-axis and color indicating the intensity of spectral counts. These are from an ISUS deployment at the C2 mooring in 2014–2015 and a SUNA deployment at the C1 mooring in 2017–2018.